NASA Technical Memorandum

NASA TM -82583

PYROTECHNIC SHOCK: A LITERATURE SURVEY OF THE LINEAR SHAPED CHARGE (LSC)

James Lee Smith

Systems Dynamics Laboratory
Science and Engineering

May 1984

National Aeronautics and
Space Administration

George C. Marshall Space Flight Center

TECHNICAL REPORT STANDARD TITLE PAGE

1. REPORT NO.	2. GOVERNMENT ACCESSION NO.	3. RECIPIENT'S CATALOG NO.
NASA TM-82583		

4. TITLE AND SUBTITLE	5. REPORT DATE
Pyrotechnic Shock: A Literature Survey of the Linear Shaped Charge (LSC)	May 1984
	6. PERFORMING ORGANIZATION CODE
7. AUTHOR(S)	8. PERFORMING ORGANIZATION REPORT #
James Lee Smith	
9. PERFORMING ORGANIZATION NAME AND ADDRESS	10. WORK UNIT NO.
George C. Marshall Space Flight Center Marshall Space Flight Center, Alabama 35812	11. CONTRACT OR GRANT NO.
	13. TYPE OF REPORT & PERIOD COVERED
12. SPONSORING AGENCY NAME AND ADDRESS	Technical Memorandum
National Aeronautics and Space Administration Washington, D.C. 20546	14. SPONSORING AGENCY CODE

15. SUPPLEMENTARY NOTES

Prepared by Systems Dynamics Laboratory, Science and Engineering.

16. ABSTRACT

The purpose of this report is to review linear shaped charge (LSC) literature for the past 20 years. The following topics are discussed:

1) LSC Configuration
2) LSC Usage
3) LSC Induced Pyroshock
4) Simulated Pyrotechnic Testing
5) Actual Pyrotechnic Testing
6) Data Collection Methods
7) Data Analysis Techniques
8) Shock Reduction Methods
9) Design Criteria

Although no new discoveries have been made in LSC research, charge shapes have been improved to allow better cutting performance, testing instrumentation has been refined, and some new explosives, for use in LSC, have been formulated. However, little progress has been made in LSC induced pyroshock.

17. KEY WORDS	18. DISTRIBUTION STATEMENT
Linear Shaped Charge (LSC) Pyroshock Reduction Methods Pyrotechnic Design Criteria Pyrotechnic Testing and Analysis LSC Usage and Configuration	Unclassified — Unlimited

19. SECURITY CLASSIF. (of this report)	20. SECURITY CLASSIF. (of this page)	21. NO. OF PAGES	22. PRICE
Unclassified	Unclassified	64	NTIS

MSFC - Form 3292 (May 1969)

For sale by National Technical Information Service, Springfield, Virginia 22151

TABLE OF CONTENTS

		Page
I.	INTRODUCTION	1
	A. Purpose	1
	B. History	1
II.	LINEAR SHAPED CHARGES	2
	A. Configuration	2
	B. Composition and Thermodynamics	4
	C. Usage	5
III.	METHODS OF PYROTECHNIC TESTING	10
	A. Simulated Testing	11
	1. Hammer Testers	11
	2. Shaker Tables	14
	3. Drop Testers	19
	4. High Intensity Shock Machines	19
	B. Explosive Testing	21
	1. Actual Flight	21
	2. Plate Testers	21
	3. Barrel Testers	21
	4. Ground Test of Flight Hardware	22
IV.	DATA COLLECTION AND ANALYSIS	22
	A. Methods of Data Collection	22
	1. Accelerometers	22
	2. Stress-Strain Measuring Devices	22
	B. Methods of Analysis	23
	1. General	23
	2. Time History	23
	3. Shock Response Spectrum	23
	4. Fourier Spectrum	33
	5. Acceleration from Strain Measurement	34
V.	METHODS OF REDUCING SHOCK OR SHOCK EFFECTS	36
	A. Shock Source Reduction	36
	B. Shock Source Isolation	36
	C. Increase Attenuation of Shocks	36
	D. Use Shock Mounts	40
	E. Modify or Redesign Equipment Receiving Shock Damage	

TABLE OF CONTENTS (Concluded)

		Page
VI.	SUMMARY OF THE "AEROSPACE SYSTEMS PYROTECHNIC SHOCK DATA" REPORT	42
VII.	PYROTECHNIC SHOCK DESIGN CRITERIA	44
	A. Types of Guidelines	44
	B. Derivation of Guidelines	44
	C. Usage	48
VIII.	SUMMARY	50
IX.	CONCLUSIONS	50
BIBLIOGRAPHY		51

LIST OF ILLUSTRATIONS

Figure	Title	Page
1.	LSC cross-sectional	2
2.	LSC cutting action	3
3.	LSC cutting action	3
4.	LSC cutting action	3
5.	LSC shape development	3
6.	LSC explosives table	4
7.	LSC target standoff	6
8.	LSC coreload performance	6
9.	LSC cutting profiles in aluminum	7
10.	LSC cutting profiles in stainless	8
11.	LSC normalized cutting profiles	8
12.	LSC penetration and cut versus coreload	9
13.	Cutting performance table	10
14.	Pendulum hammer test apparatus	11
15.	Pendulum hammer test apparatus	12
16.	Pendulum hammer test instrumentation	12
17.	Pendulum hammer shock transient	13
18.	Pendulum hammer Fourier spectrum	13
19.	SRS - X direction	13
20.	SRS - X direction	13
21.	SRS - Y direction	14
22.	SRS - Z direction	14
23.	Vibration table shock input	15
24.	Spacecraft shock Z axis	15
25.	Spacecraft shock X axis	16

LIST OF ILLUSTRATIONS (Continued)

Figure	Title	Page
26.	Spacecraft shock Y axis	16
27.	Spacecraft shock Z axis	17
28.	Vibration table shock Y axis	17
29.	Vibration table shock X axis	18
30.	Summary pyrotechnic shock data	19
31.	Standard drop machine configured for pyroshock	20
32.	Repeatability of ten pyrotechnic shocks	20
33.	Barrel tester	22
34.	SRS - theoretical bounds and data	24
35.	SRS - actual data	24
36.	SRS - data	25
37.	SRS - data	25
38.	Acceleration time history	26
39.	SRS	26
40.	Acceleration time history	26
41.	SRS	26
42.	Comparison of SRS at various propagation distances	27
43.	Effect of frequency increment on shock spectrum amplitude	27
44.	Mechanical test system	29
45.	Instrumentation system	29
46.	Four shock spectra comparing effects of various sources	30
47.	A comparison of three forms of data	31
48.	Dynamic model for longitudinal impact	31
49.	Transmitted and reflected stress waves	31
50.	Calculated and measured time histories	31

LIST OF ILLUSTRATIONS (Continued)

Figure	Title	Page
51.	Simple dynamic impact	32
52.	Shock spectra from simple dynamic impact	32
53.	Two forms of shock spectra	32
54.	Fourier spectrum - SRS plots	33
55.	Time histories	35
56.	Time histories	35
57.	Test apparatus	37
58.	Joint configuration	37
59.	Insert materials table	37
60.	Shock reduction table	38
61.	SRS data	39
62.	SRS data	39
63.	SRS data	39
64.	SRS data	39
65.	SRS data	39
66.	SRS data	39
67.	Test component	40
68.	SRS envelope	40
69.	Isolation washer table	41
70.	Shock reduction table	41
71.	SRS data	41
72.	SRS data	41
73.	Shock reduction versus frequency	41
74.	MSS shroud separation data	43
75.	MSS shroud separation data	44

LIST OF ILLUSTRATIONS (Concluded)

Figure	Title	Page
76.	Attenuation versus distance from source	45
77.	Attenuation for various joints	46
78.	Attenuation for various joints	46
79.	Data analysis methods	47
80.	Predicted SRS	47
81.	Attenuation for cylindrical shell	48
82.	Predicted SRS	49

TECHNICAL MEMORANDUM

PYROTECHNIC SHOCK: A LITERATURE SURVEY OF THE LINEAR SHAPED CHARGE (LSC)

I. INTRODUCTION

A. Purpose

One of the least understood aerospace problems is pyrotechnic shock. The purpose of this report is to summarize research, on the linear shaped charge (LSC) and its associated pyrotechnic shock, for the past 20 years. Also, problems associated with LSC pyroshock will be discussed and solutions will be suggested. Simulation and testing methods, design guidelines, and other appropriate information will be included.

B. History

Before Christ's birth, the Chinese used the first pyrotechnic device: fireworks [90]. In the year 1500, technologists began to use the word pyrotechnics, from the Greek words pyr (fire) and techne (art, skill) [81:5], to describe the use of fire for metal smelting and the heating and pickling of materials in manufacturing [8:2].

The first pyrotechnics text, "De Pirotechnia," was published in 1540 by a Venetian named Vannocchio Biringuccio.

In today's usage, pyrotechnics refers to incendiary, detonating, smoke-generating, and explosive devices.

In this report, pyrotechnics will be limited to linear-shaped charge explosive cutting devices. LSC uses the Munroe Effect to cut metal.

C. E. Munroe (1849-1938), a U.S. chemist, discovered the so-called Munroe Effect, stated as follows: "The Munroe Effect is the reinforcement of shock waves in a hollow charge, concentrating the effect of the explosion along the axis of the charge" [73].

In recent years, LSCs have been used extensively in the aerospace industry. The shock environments produced by LSCs can cause damage and even failure of the surrounding attached structure, as well as other components mounted upon that structure. Shock is a transient phenomenon. It is measured as an event time history.

Pyrotechnic shock is the least understood of the dynamic environments associated with the operation of aerospace vehicles. Pyroshock continues to be a problem for testing and designing aerospace structures. In random vibration, the dynamicist can perform a response analysis for an item and then produce a set of load factors for design and stress engineers to use in equipment design. However, in pyrotechnic shock, definition of the environment is still an empirical procedure. Prediction and explanation of pyrotechnic shock environments have defied vigorous mathematical solution.

II. LINEAR SHAPED CHARGES

This section is an overview of LSCs, their characteristics, and how they perform. LSCs must be understood before the principles of the heart of this paper (LSC induced pyrotechnic shock) may be grasped.

A. Configuration

Linear shaped charges are composed of a seamless metal sheath containing an explosive core. A "V" configuration is used for all modern LSCs. The continuous liner and explosive produce a linear cutting action. The Munroe Effect is enhanced by careful control of charge dimensions and configuration. Figure 1 is a cross-sectional view of an LSC [2:II-1 to II-34].

The main use of LSCs is the cutting of metal in separation systems. When fired, the V-shaped cavity causes angular convergence of combined shocks to form a higher intensity shock wave. This concentration of explosive force, the "Munroe Effect," can be further enhanced by lining the cavity with metal. Thus, a jet of metallic particles, having velocities sometimes greater than the explosive detonation velocity, is found [25:2-31].

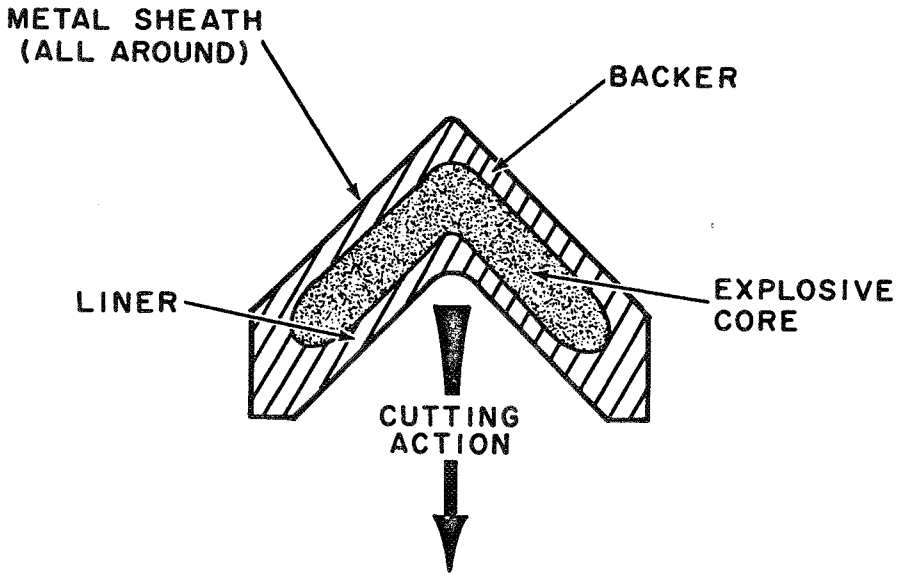

Figure 1. LSC cross-sectional.

Figures 2, 3, and 4 illustrate how an LSC produces a liquid metal cutting jet. Notice that the jet penetrates the target approximately 50 percent and that shock-induced cracking accounts for the remaining 50 percent of the total cut [50:4].

The first LSCs were made in the 1950's. These were kidney-shaped. Through the years, LSCs have evolved to the presently used configurations IV and V as in Figure 5 [22: II-1 to II-34].

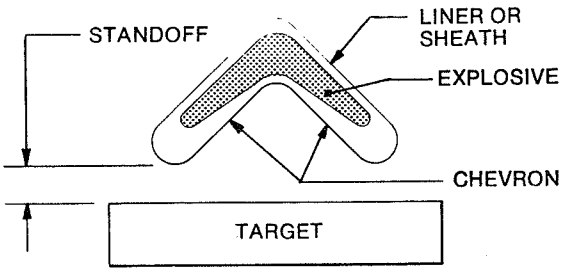

Figure 2. LSC cutting action.

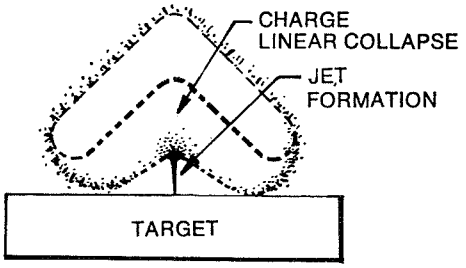

Figure 3. LSC cutting action.

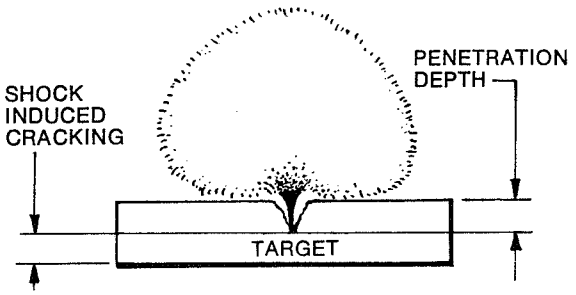

Figure 4. LSC cutting action.

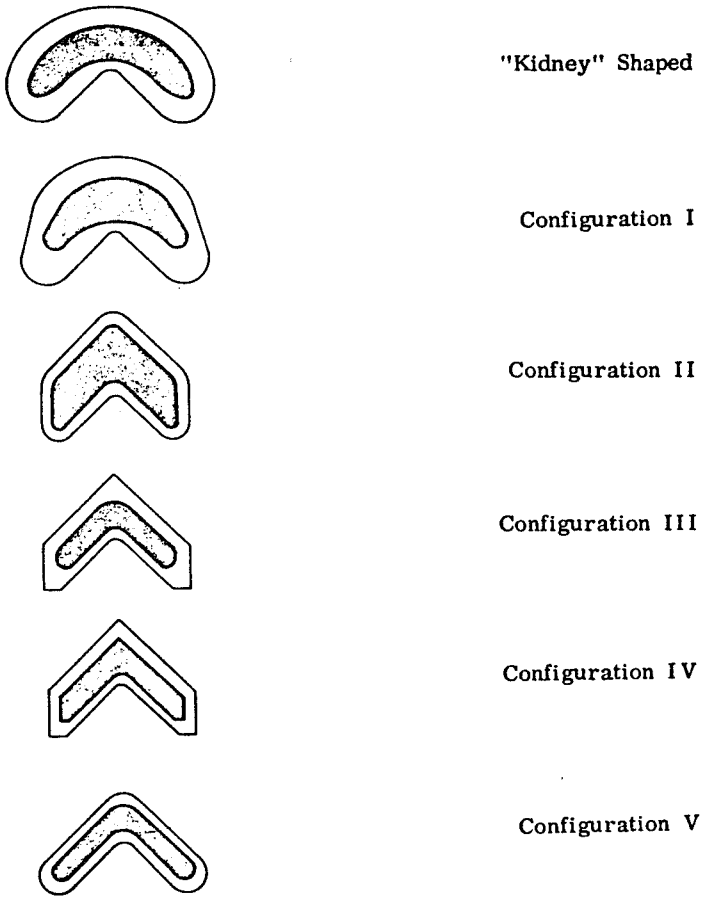

Figure 5. LSC shape development.

B. Composition and Thermodynamics

Metal sheaths are usually made from lead, aluminum, copper, or silver. Lead LSCs are flexible while the others are stiff. Aluminum weighs less than lead in LSCs of the same core load. Thus, aluminum is more effective on a weight-to-weight basis. However, more standoff (distance from LSC to surface to be cut) is required with aluminum. Increased standoff requires additional structural weight but yields reduced structural shock loads. Silver is a "specialty" and is rarely used. Copper sheaths produce the maximum cut for the amount of explosive. Copper sheath LSCs are used on the Space Shuttle [22: II-1 to II-34].

Five varieties of explosive are in common use. Other varieties are used in "specialities" and will not be mentioned here. Cyclotrimethylenetrinitramine (RDX), a colorless explosive, is usually dyed pink for use in LSCs. RDX must be highly purified to insure stability at higher temperatures. Most LSCs contain RDX.

Cyclotetramethylenetetranitramine (HMX) is very similar to RDX. HMX is white to colorless. It may be used at higher temperatures than RDX.

Pentaerythritoltetranitrate (PETN) is less powerful and more sensitive than RDX. PETN is used primarily in detonators, but may be used in LSCs.

Dipicramide (DiPam) is a new explosive developed by the Naval Ordnance Laboratory (NOL). It is less brisant and less sensitive than RDX.

Hexanitrostilbene (hNs) is a new explosive also developed by NOL for high temperature applications.

Figure 6 summarizes the properties of the five explosive varieties.

	RDX	HMX	PETN	DI PAM	HNS
SPECIFICATION	MIL–R–398	MIL–H–45444	MIL–P–387	WS–4660(NOL)	WS–5003D (NOL)
MELTING POINT	190°C	273°C	141°C	304°C	316°C
AUTOIGNITION	405°C	380°C	272°C	MELTS	MELTS
DETONATION RATE	8200 M/S AT 165 g/cm^3	9100 M/S AT 1.84 g/cm^3	8300 M/S AT 1.7 g/cm^3	7130 M/S AT 1.6 g/cm^3	6900 M/S AT 1.6 g/cm^3
MAXIMUM PROLONGED STORAGE TEMP.	250°F	300°F	160°F	–	–
COLOR	CLEAR, DYED PINK	WHITE TO CLEAR	–	YELLOW CRYSTALLINE	PALE YELLOW NEEDLES
DEGRADATION	350°F AFTER 1/2 HR.	425°F AFTER 1/2 HR.	250°F AFTER 1/2 HR.	–	–
	325°F AFTER 1 HR.	400°F AFTER 1 HR.	225°F AFTER 2 HR.		
	300°F AFTER 4 HR.	375°F AFTER 4 HR.	200°F AFTER 4 HR.		
CRYSTAL DENSITY	–	–	–	1.79 g/cm^3	1.75 g/cm^3

Figure 6. LSC explosives table.

C. Usage

Linear shaped charges are used primarily for cutting purposes such as in separating boosters, cutting skirts, etc. Metals, tubing, wire bundles, ablative material, composite honeycomb, fiberglass reinforced laminates, nylon strapping, and other materials may be cut by LSCs [22 II-1 to II-34].

LSC cutting ability is a function of detonation rate and sheath material characteristics. Cutting ability is affected by hardness, strength, and density of the material being cut. Penetration and cut are related to coreload as follows:

$$\frac{T_1}{T_2} = \left(\frac{W_1}{W_2}\right)^{0.6}$$

where T_1 and T_2 are the total cut of a given material and W_1 and W_2 are coreloads.

Penetration usually accounts for one-half of the total cut with fracture accounting for the remainder of the cut.

LSC manufacturing companies have performed extensive testing to determine cut as a function of coreload for various metals to be cut. Cutting depth is also a function of standoff (distance from charge to surface to be cut) (Fig. 7). Figure 8 illustrates cut versus coreload for lead sheathed RDX with zero and recommended standoff.

Figure 9 illustrates standoff versus cut depth in aluminum for a lead/RDX LSC for various coreloads. Figure 10 is the same as Figure 9 except it is for stainless steel.

Figure 11 illustrates percent cut as a function of standoff.

Similar design guidelines are available for other sheath and explosive varieties of LSC. Figure 12 is for lead/RDX cutting stainless or aluminum at recommended standoff. Coreload versus cut is plotted.

References 19, 22, 23, and 50 all contain much of the same information. Reference 22 was used more often, in this paper, than the others simply because it was published more recently.

Tables are available from manufacturers listing recommended standoff for each variety and coreload to LSC. Figure 13 is an example.

A "Catalog of European Pyrotechnic Devices for Use in Space" is available from the European Space Agency (ESA). Section 10-D of this catalog lists linear-shaped charges and their characteristics (cutting ability, size, coreload, thermal qualities, etc.) [10:10-D; 11:10-D]. Bouloumie and Garage discuss uses of pyrotechnics in the ESA Ariane launch vehicle. Included is a summary of technical design criteria as well as system design control procedures [14:339]. Lemay presents the characteristics of pyrotechnic devices and the conditions under which they are used in space [41]. Bement discusses quality control of pyrotechnics [9]. Variations in pyrotechnic devices may account for variations in the shock produced.

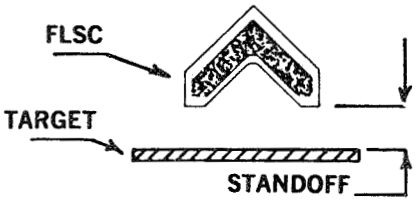

Figure 7. LSC target standoff.

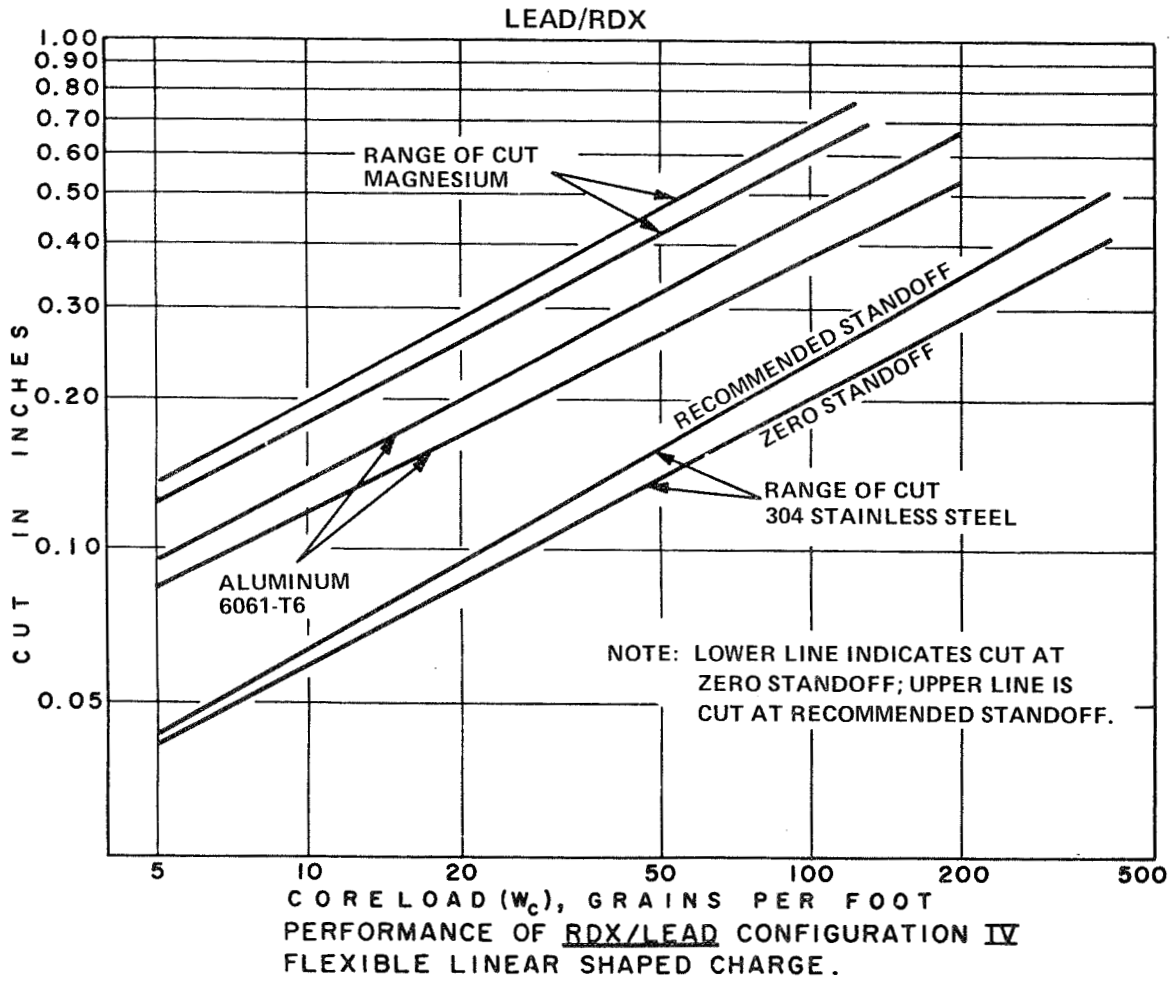

Figure 8. LSC coreload performance.

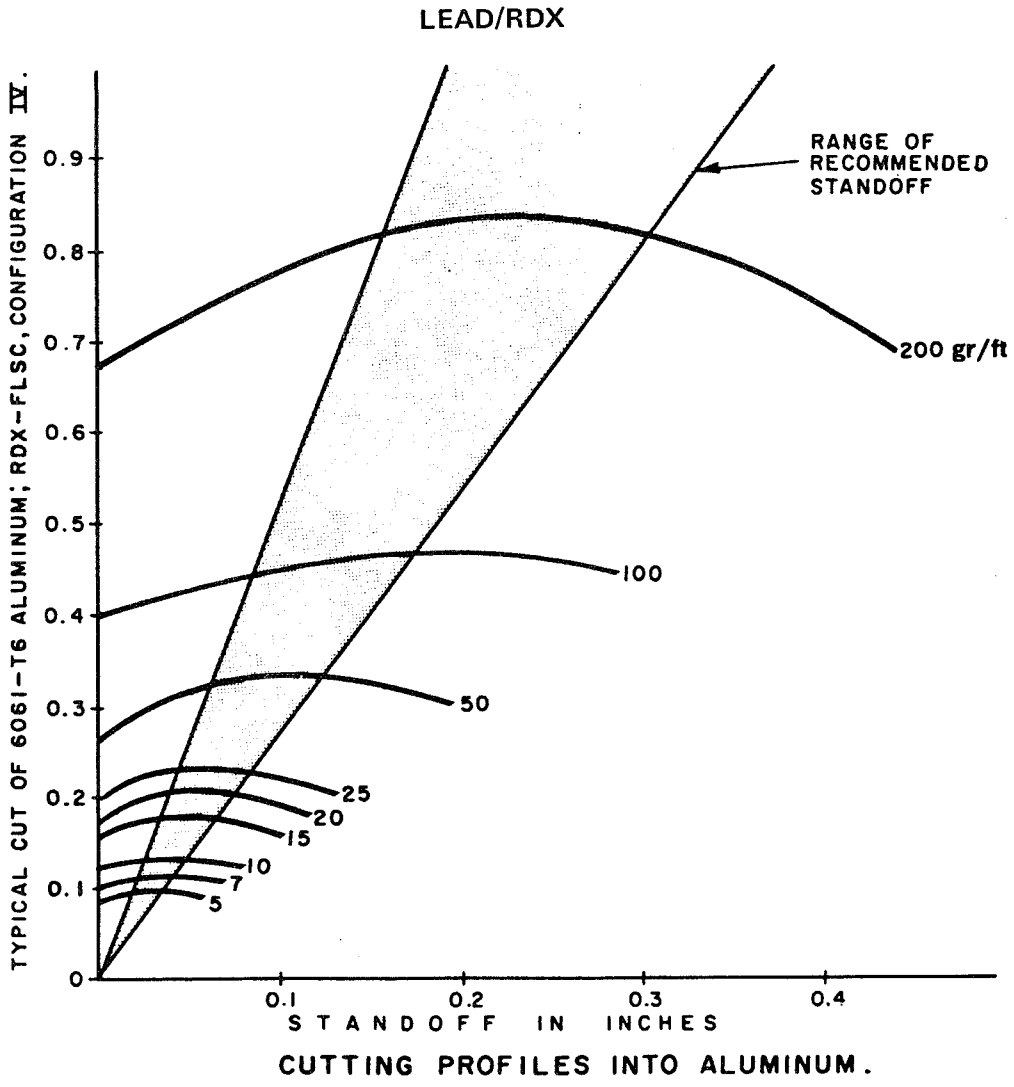

Figure 9. LSC cutting profiles into aluminum.

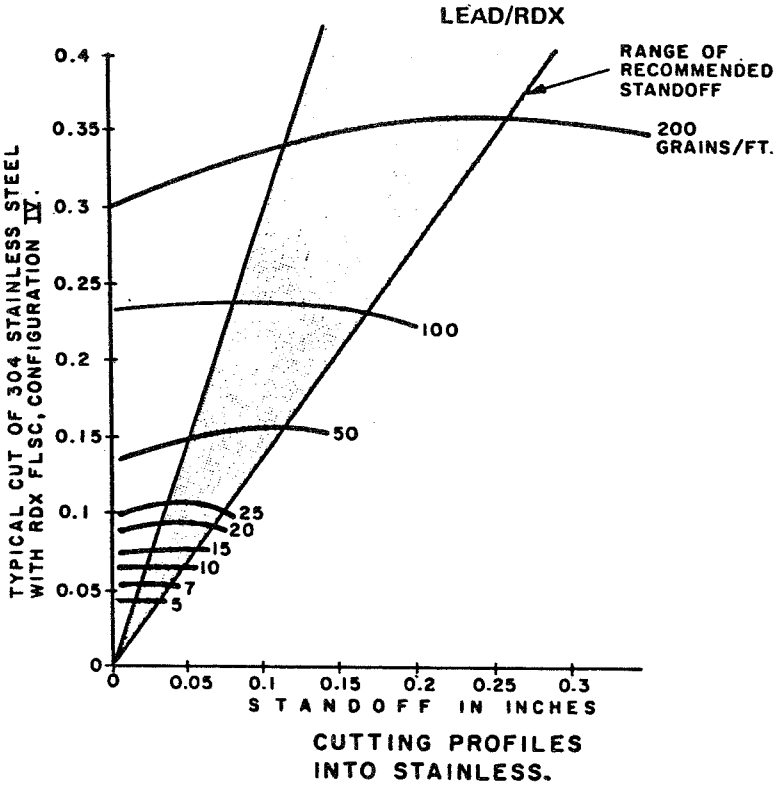

Figure 10. LSC cutting profiles into stainless.

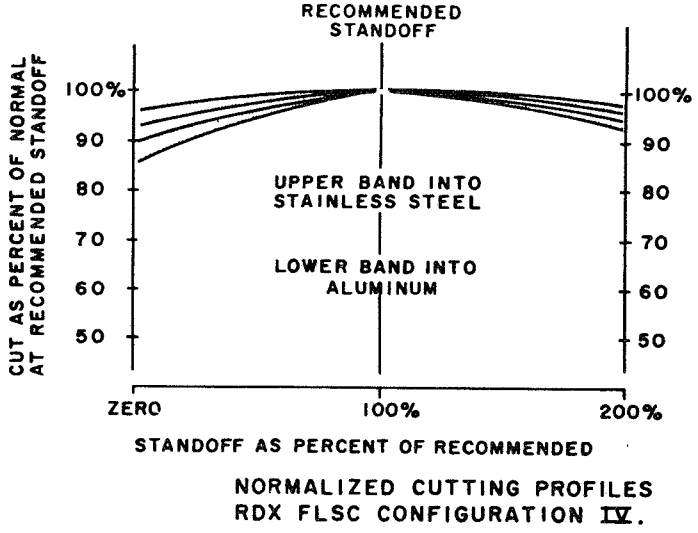

Figure 11. LSC normalized cutting profiles.

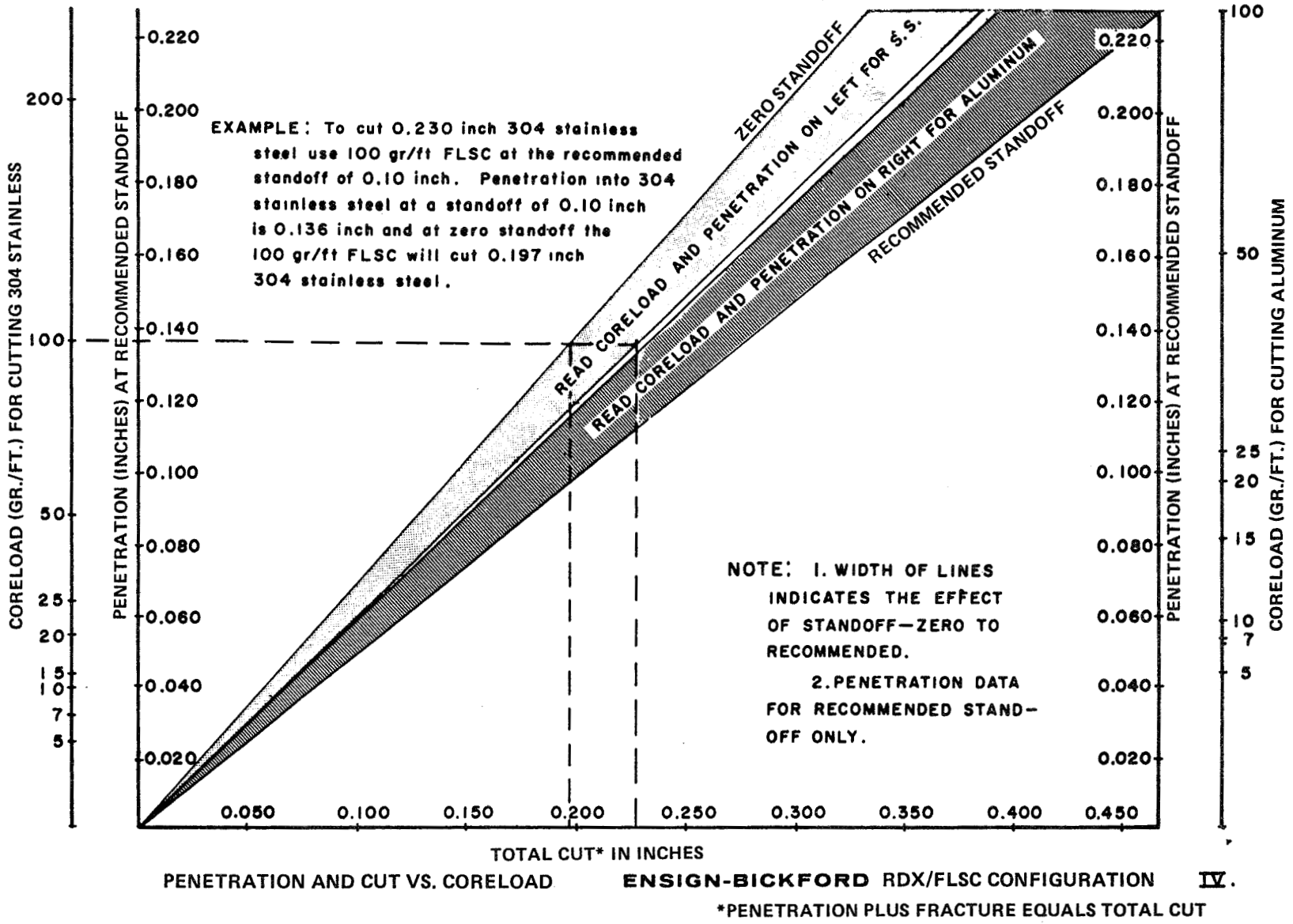

Figure 12. LSC penetration and cut versus coreload.

Papers by Falbo and Robinson [26], Brauer [12], and Simmons [82, 83], all discuss Apollo spacecraft pyrotechnics.

The use of LSC in the Space Shuttle is discussed by Lake, Thompson, and Crexelius in their article in the proceedings from the "Conference of Modern Applications of Pyrotechnics" [15]. Design and flight performance of Space Shuttle separation pyrotechnics are detailed by Rogers in "Space Shuttle Separation Mechanisms" [76]. The proceedings of the "Fifth International Pyrotechnics Seminar" contain information on Space Shuttle pyrotechnics [68:503-521]. Graves has two papers on the same topic [14:263-70; 29:263-269].

Nominal Core Load (gr/ft)	E-B P/N and Dwg. Ref.	Recom'd Stand-off (s/o)	Cutting Performance					
			Against Aluminum (1)			Against Stainless Steel (2)		
			Zero s/o	Rec'd s/o	150% s/o	Zero s/o	Rec'd s/o	150% s/o
3	206083							
5	206013	0.030	0.085	0.096	0.092			
		0.020				0.042	0.043	0.042
7	206003	0.045	0.100	0.110	0.097			
		0.024				0.052	0.055	0.053
10	206027	0.045	0.120	0.125	0.124			
		0.010				0.065	0.065	0.065
15	206002	0.045	0.155	0.174	0.168			
		0.045				0.072	0.077	0.075
20	206016	0.045	0.165	0.208	0.202			
		0.045				0.085	0.095	0.093
25	206008	0.045	0.183	0.227	0.222			
		0.045				0.090	0.107	0.100
50	206007	0.100	0.260	0.337	0.328			
		0.100				0.132	0.156	0.151
100	206006	0.180	0.392	0.465	0.450			
		0.100				0.233	0.238	0.234
200	206009	0.230	0.665	0.830	0.790			
*		0.230				0.300	0.360	0.348

(1) 6061-T6-Al, inches cut.
(2) 304 stainless, inches cut.

Figure 13. Cutting performance table.

III. METHODS OF PYROTECHNIC TESTING

Terminology such as shock response spectrum (SRS) and others will be discussed in detail in Section IV.

Varieties of shock machines are drop testers, pendulum hammers, and high intensity shock machines (sling shots and pressure driven impact machines). Shock machines usually produce simple pulses and are not capable of producing complex pulses such as pyroshocks. Also, shock machines are limited to small test items. The simple unbalanced acceleration produces a velocity shock which may result in a severe overtest in low frequency but an undertest in high frequency. Rigid shock tables are not characteristic of aerospace structures. However, shock machines are low cost and they produce the required SRS [31:45].

Electrodynamic shakers also usually produce simple pulses (there are exceptions). Shakers have about the same qualities as shock machines but can test larger items [31:45-48].

The best method of pyrotechnic testing, however, is still achieved by using a pyrotechnic source. Smith summarizes methods of specifying and performing tests to determine effects of pyroshock on structures [85].

A. Simulated Testing

"Pyrotechnic Shock Testing - Past and Future" by H. N. Luhrs, discusses the history of shock testing, especially testing methods. Pyrotechnic shock is a very high frequency, high acceleration transit which usually decays in less than 20 milliseconds. Most pyroshock failures occur as electrical shorts or fractures of crystal or alumina substrates [45].

Papers on pyrotechnic shock testing were presented at "Environmental Technology '76." Equipment failure, modes, test configuration, and other facets of testing were considered [24, 91].

1. Hammer Testers

A given pyrotechnic shock response spectrum is not unique to a given shock transient. That is, more than one shock transient can produce the same shock spectrum. Therefore, drop tables, shaker tables, and other methods can be used to produce shock response spectrums equivalent to explosively produced spectrums. One method is the high g, metal-to-metal pendulum hammer resonant test fixture illustrated in Figure 14 [4].

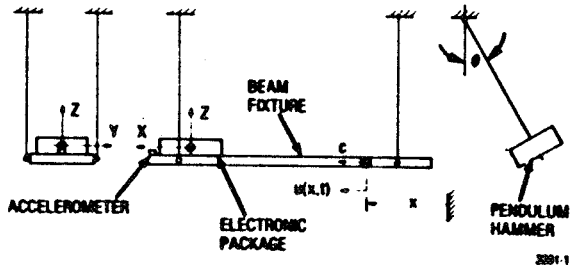

Figure 14. Pendulum hammer test apparatus.

This fixture is used to pyroshock test electronic packages. The impulsive load generating pendulum hammer is a 13 lb steel block. The aluminum beam measures 48 x 6 x 1 in. The aluminum plate is 17 x 10 x 3 in. The length (L) of the resonant beam is determined by the following equation.

$$L = \frac{C}{2f_1}$$

where C is the speed of the dilatational wave in the beam and f_1 is the fundamental beam frequency.

The harmonic frequencies (f_N) are determined as follows:

$$f_N = \frac{NC}{2L}$$

where N = 1, 2, 3, ...

The beam is used to test in the X and Y directions and the plate is used for the Z direction. Figure 15 shows the Z axis test setup.

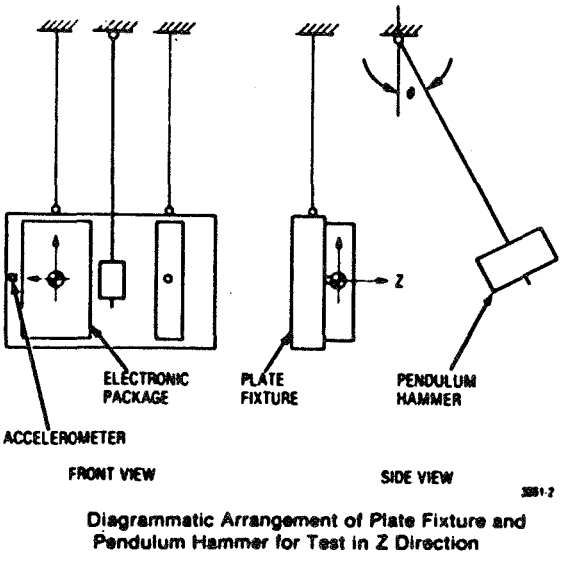

Figure 15. Pendulum hammer test apparatus.

Shock transients were measured by an accelerometer, amplified, and then analyzed by a digital computer (Fig. 16).

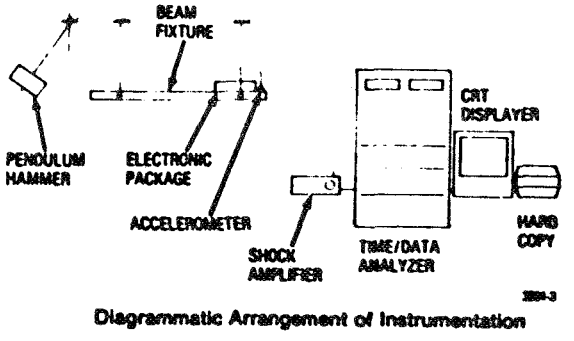

Figure 16. Pendulum hammer test instrumentation.

A typical X axis acceleration time history and Fourier spectrum are illustrated in Figures 17 and 18.

Figures 19 through 22 show the shock response spectrums for one test in the X axis, then for multiple tests in the X, Y, and Z axes. The solid line is the predicted spectrum and the dotted lines are tolerances or tolerance envelopes as per military standard.

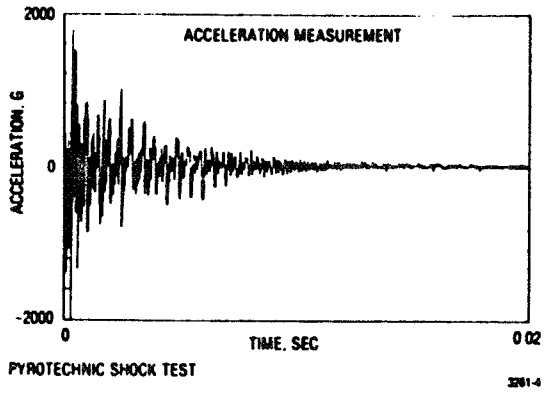

Shock Transient Measured in X Direction

Figure 17. Pendulum hammer shock transient.

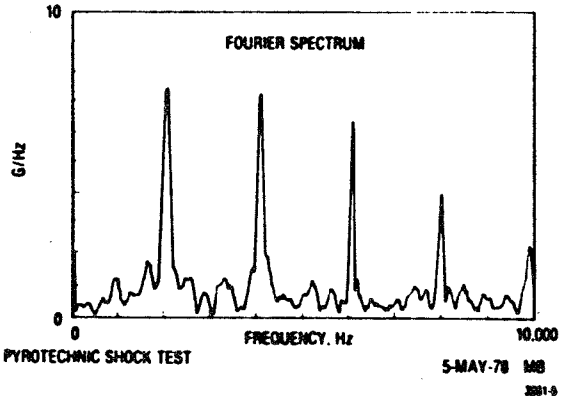

Fourier Amplitude Spectrum of Shock Transient Measured in X Direction

Figure 18. Pendulum hammer Fourier spectrum.

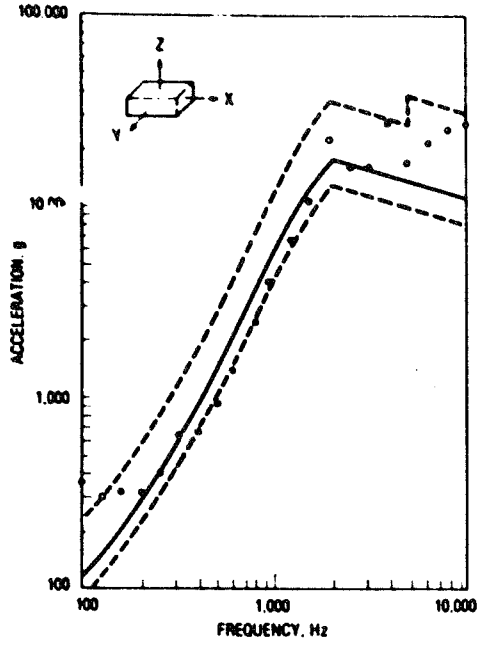

Shock Response Spectrum of Shock Transient Measured in X Direction

Figure 19. SRS-X direction.

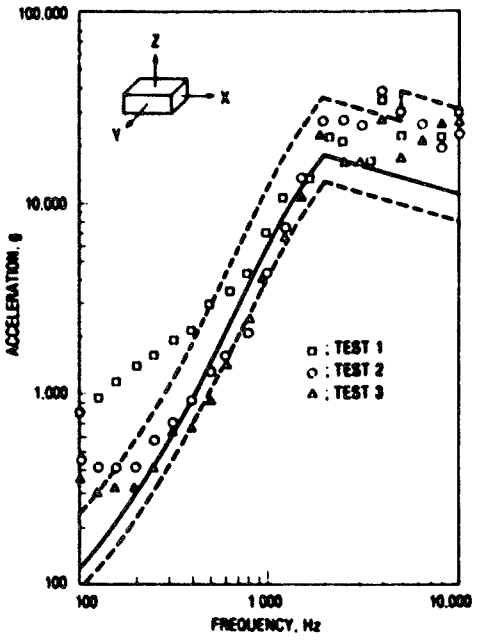

Shock Response Spectra of Tests in X Direction

Figure 20. SRS-X direction.

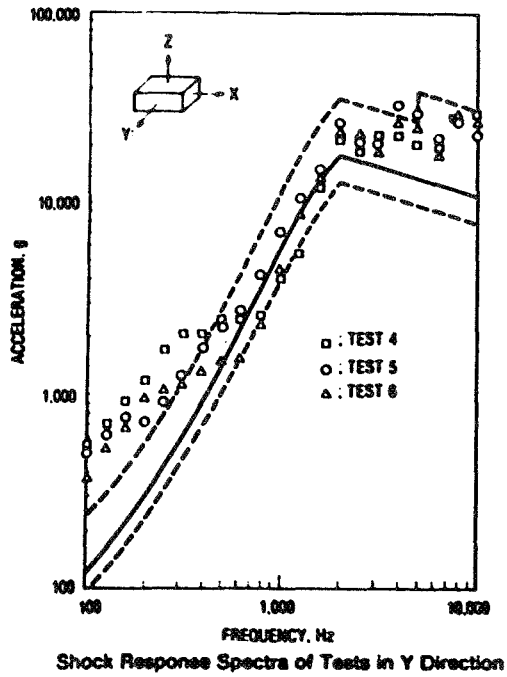

Figure 21. SRS-Y direction.

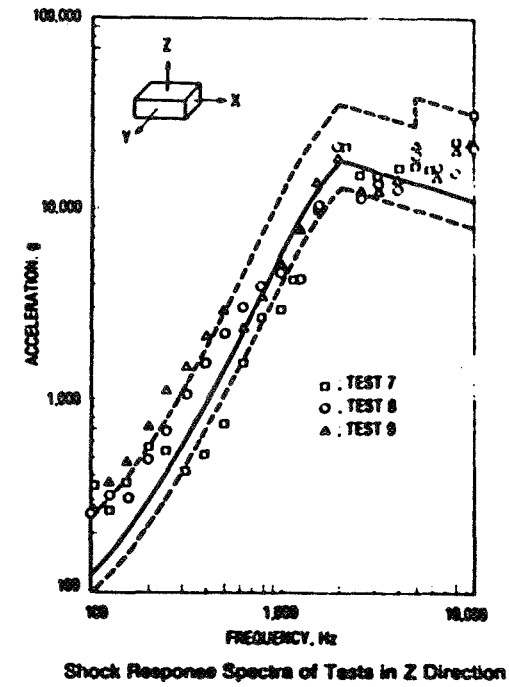

Figure 22. SRS-Z direction.

2. Shaker Tables

Pyroshock testing on hard-mounted fixtures can produce extremely high acceleration levels, higher than those measured on actual spacecraft structure, this producing unrealistic response levels inside the equipment being tested. Therefore, any test criteria used in qualification should be carefully reviewed before initiation of the program. If possible, use representative spacecraft structures instead of shaker tables [16].

Conway and Sereno have demonstrated that testing on a representative spacecraft structure is more reliable and accurate than testing on a rigid test fixture such as a shaker table.

In "Pyrotechnic Shock Transmission in Component Versus S/C Testing," H. N. Luhrs summarizes the results of a study to compare pyroshock testing using a shaker table versus actual spacecraft pyroshock. The original purpose of the study was to determine crystal failure potential as crystals are very shock sensitive. A "black box" containing 1188 crystals was used as a test model in both tests. In the spacecraft, the "box" was mounted to a honey-comb panel; while in the shaker test, the "box" was mounted directly to a rigid mounting plate. Twenty-eight accelerometers were used [46:27-46].

A sine sweep was conducted to locate resonant frequencies. Then a shock input spectrum was derived, based on empirical design criteria, to simulate a pyrotechnic charge. Figure 23 illustrates the input spectrum. Solid lines are the input envelope, while X denotes the actual test input. The peak spectrum is 2500 g's.

Figures 24 through 29 illustrate SRS for each axis obtained from actual spacecraft firing and from the shaker test using the given input criteria. Results: The spectrums inside the black box were lower during actual spacecraft pyrotechnic shock

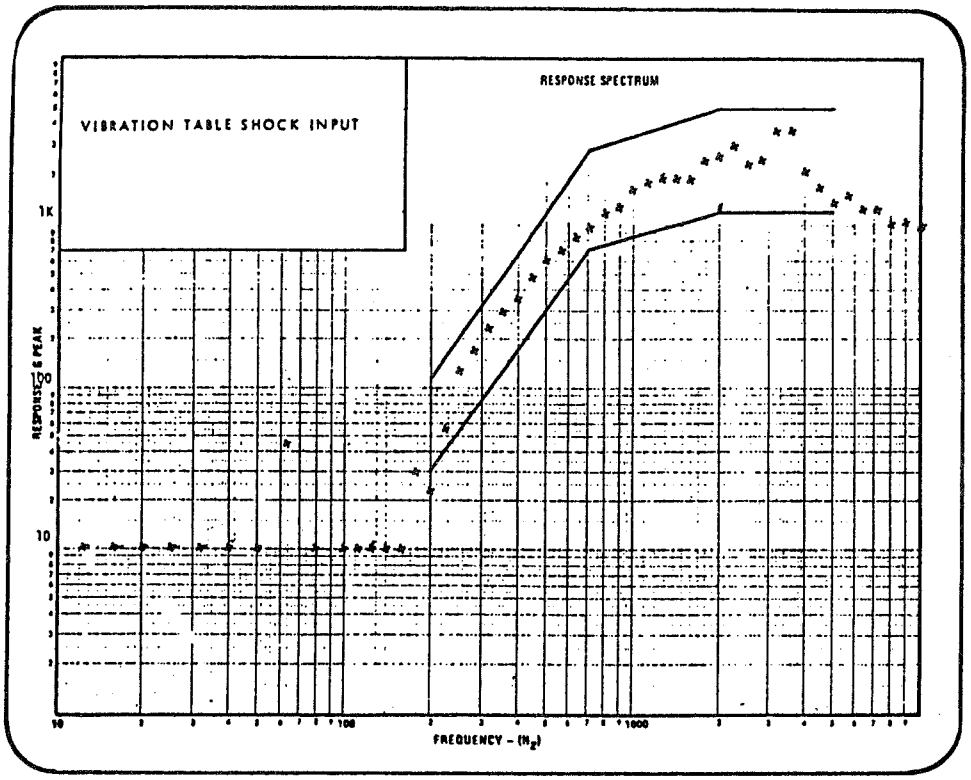

Figure 23. Vibration table shock input.

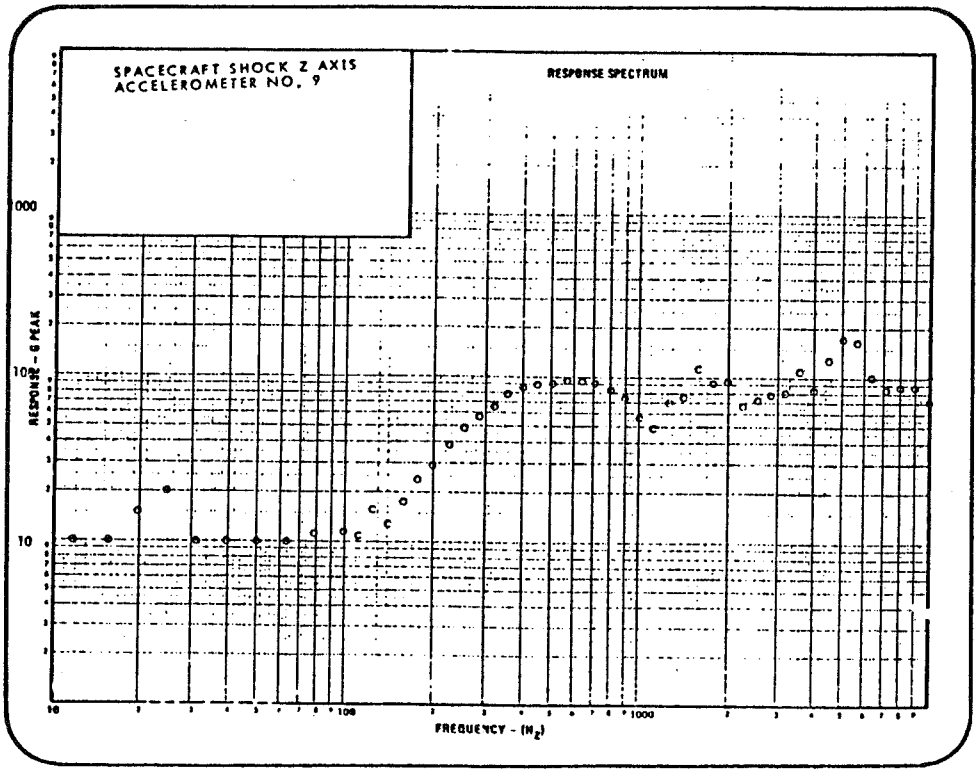

Figure 24. Spacecraft shock Z axis.

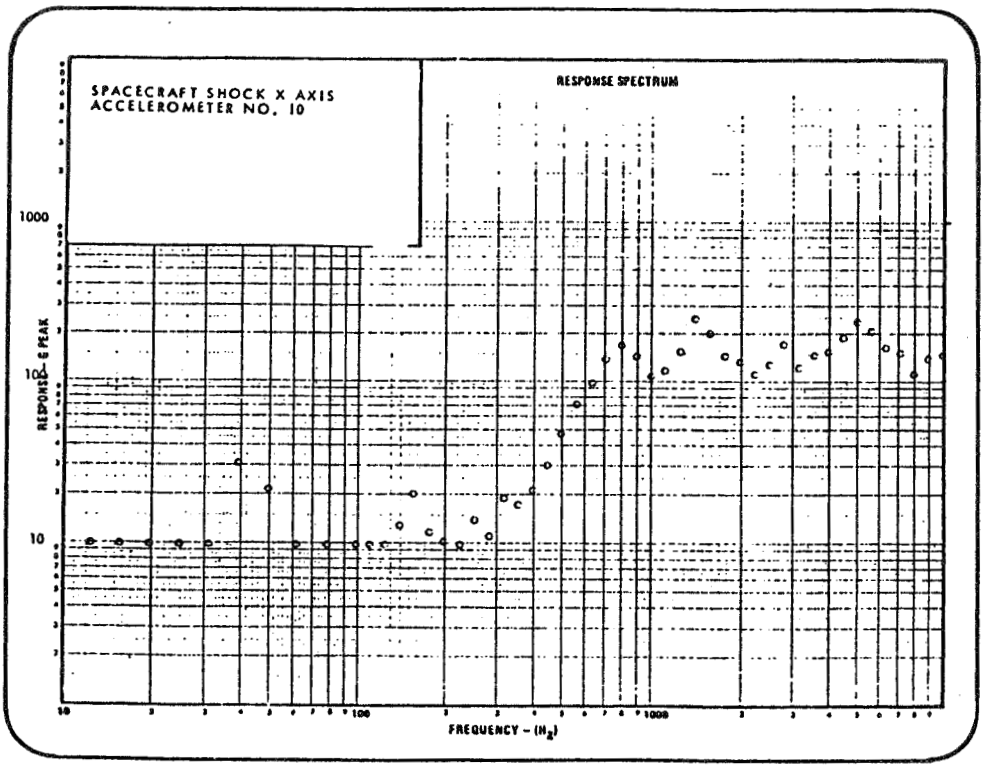

Figure 25. Spacecraft shock X axis.

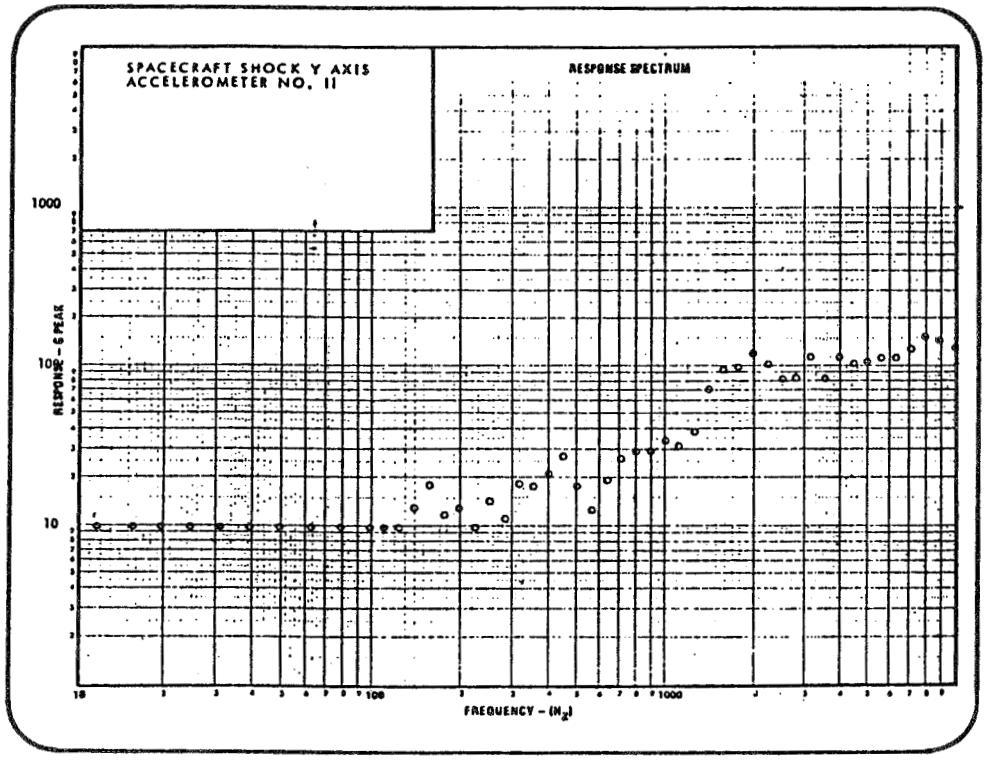

Figure 26. Spacecraft shock Y axis.

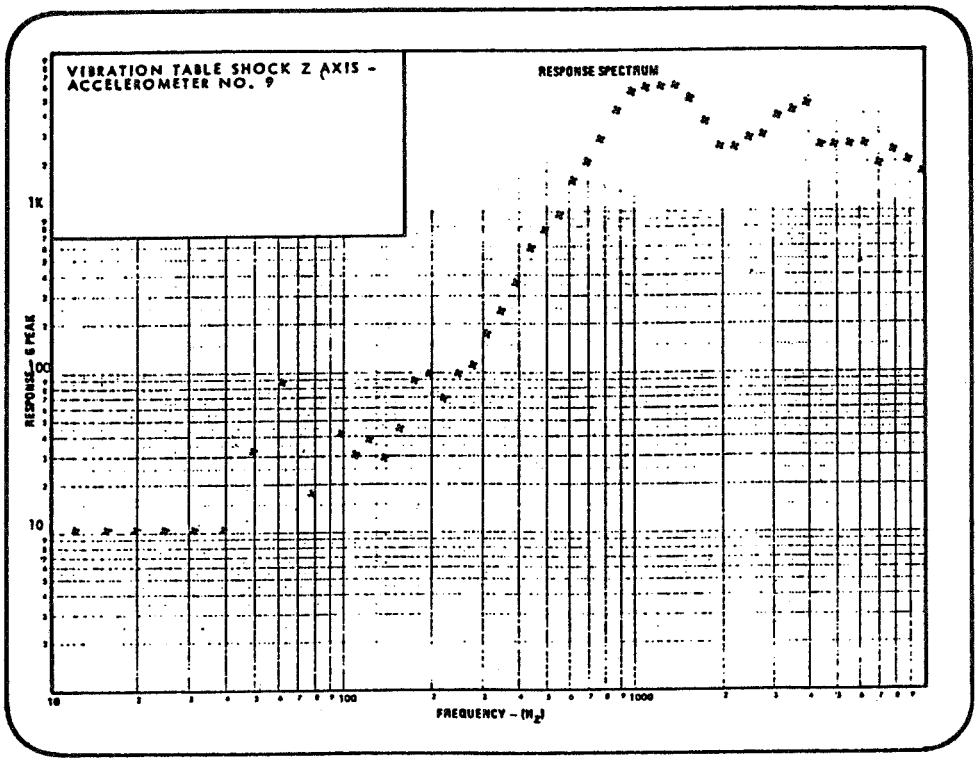

Figure 27. Spacecraft shock Z axis.

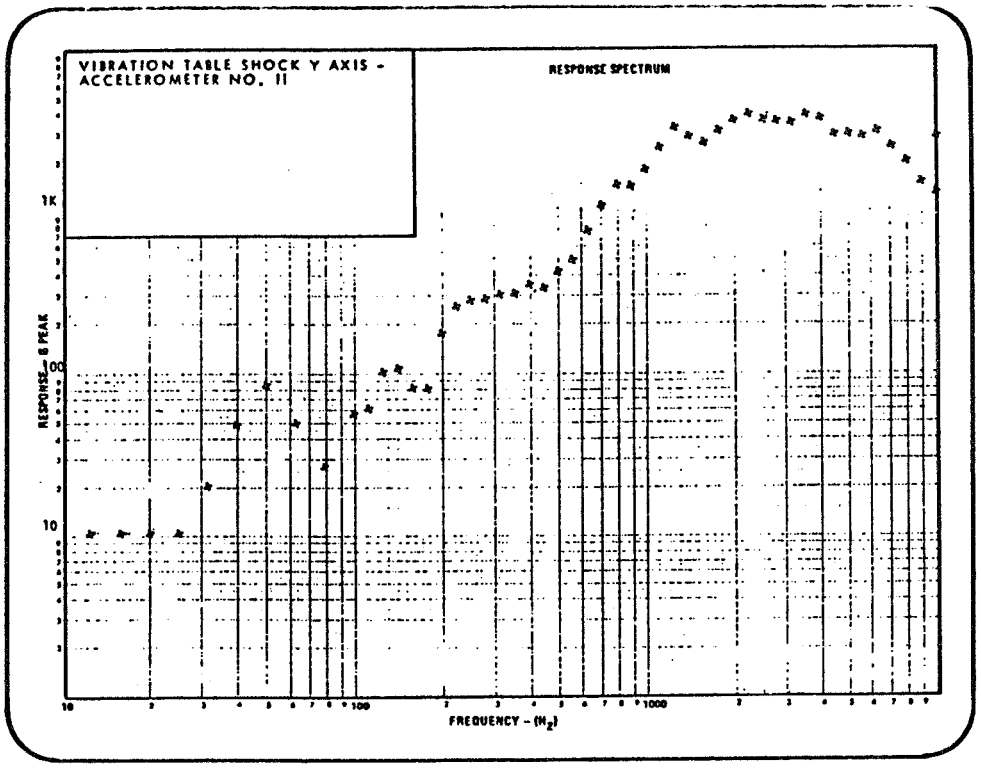

Figure 28. Vibration table shock Y axis.

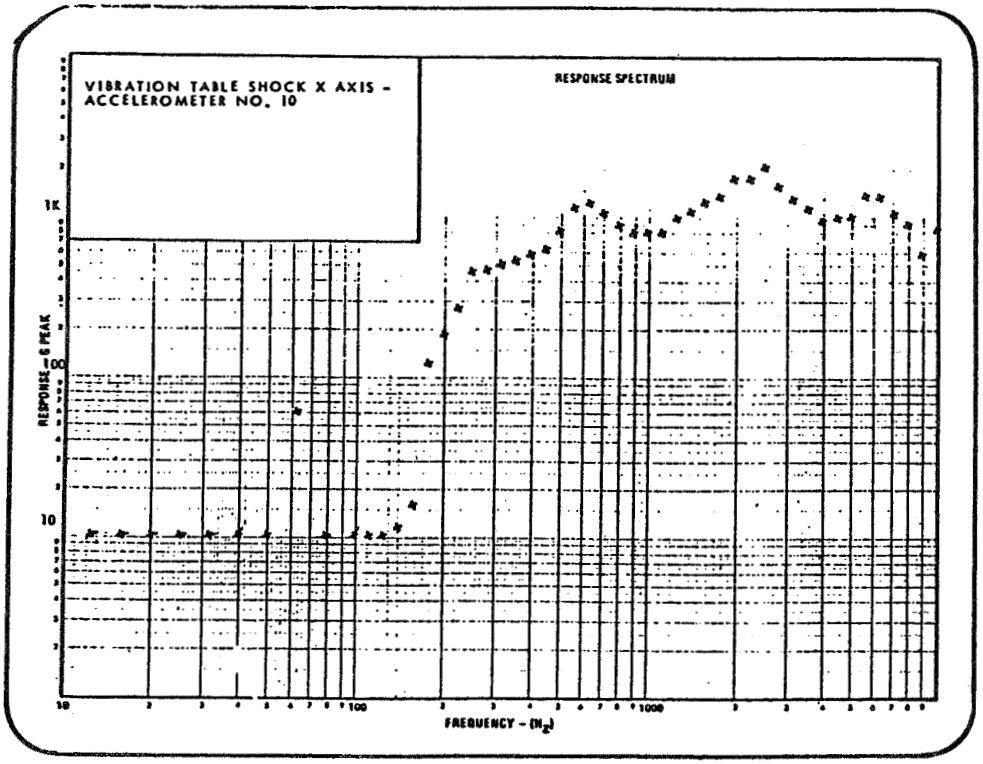

Figure 29. Vibration table shock X axis.

than during vibration table shock. Figure 30 gives numerical data from each accelerometer. These tests illustrate one of the major pyroshock testing problems: the simulation or shaker table test was a severe overtest even though the initial input SRS matched the actual pyroshock SRS.

Larue and others have developed a pyrotechnic pulse generator to use in inflight shock testing [40]. Another method of testing is to generate a nonstationary transient by modulating a stationary broad band random signal with an exponentially decaying pulse. This transient simulates a pyrotechnic transient [13].

A new electromagnetically-driven explosive shock simulator (EDESS) is being used at the Naval Surface Weapons Center. EDESS-1 can test a payload up to two metric tons. Spiral-pancake magnets produce a magnetic repulsive force between a large reaction mass and a smaller load mass. Computer controls operate the system much like a standard shaker table; however, much larger loads can be tested [78].

Schumacher has designed a three-dimensional vibration fixture. This cube-shaped fixture reduces test time to 1/3 that previously required. Three test units can be tested at a time. Test units are rotated on the second and third runs to complete triaxial testing [80].

Albers and Milder have developed a miniature pyroshock simulator (shaker device) for onboard usage in spacecraft [55].

SUMMARY PYROTECHNIC SHOCK DATA

ACCEL NO.	AXIS	S/C ACTUAL PYROTECHNIC SHOCK SPECTRUM G LEVEL G PEAK	FREQ. PEAK HZ	MAX. PEAK	PEAK 1-3K Hz REGION	AVE. 1-3K Hz REGION	HARD MOUNT TEST (2500 g) G PEAK	SPECTRUM G LEVEL FREQ. PEAK HZ	MAX. PEAK	PEAK 1-3K Hz REGION	AVE. 1-3K Hz REGION
1	X	190	3500	1100	500	250	650	3200	2800	2500	1500
2	Y	195	8000	1200	500	200	3000	9000	5500	5000	3500
3	Z	190	3500	700	450	300	1500	1600	4000	4000	3500
4	Z	200	10K	850	250	180	VOID	VOID	VOID	VOID	VOID
5	X	130	900	480	380	300	1200	1200	4000	4000	3000
6	Y	65	2000	280	280	150	VOID	VOID	VOID	VOID	VOID
7	Z	60	2000	320	320	200	----	1400	4000	4000	2500
8	Z	100	3500	390	200	130	----	2800	5200	5200	4000
9	Z	55	5000	170	120	90	1700	1200	6000	6000	4000
10	X	90	1400	250	250	150	600	2500	2100	2100	1500
11	Y	70	8000	150	120	100	1300	2200	4000	4000	3000
12	Z	90	5000	260	140	110		1400	4600	4600	3000
13	Y	120	5500	480	120	90	1600	8000	6500	2800	2000
14	X			VOID			700	2000	3100	3100	2000
15	X	150	1100	450	450	300	1200	2000	5300	5300	3000
16	Y	70	2800	320	320	200	800	2200	3300	3300	2000
17	Y	130	3600	600	320	200	1600	1800	5000	5000	3000
18	X			VOID			VOID	VOID	VOID	VOID	VOID
19	Y	80	6200	380	220	180	1000	9000	2900	2500	2000
20	Z			VOID			1800	1400	6000	6000	4500
21	X	390	6200	1800	500	350					
22	Y	330	8800	1100	480	300					
23	Z	400	2300	1200	1200	1000					
24	Z	300	6400	1000	750	550					
25	Z	270	1300	520	520	400					
28	Z	800	1600	2700	2700	1600					

Figure 30. Summary pyrotechnic shock data.

3. Drop Testers

Drop testing machines impart a velocity change to the test item. Pyrotechnic devices such as LSCs do not impart velocity change to a missile body, therefore, drop testing is not very adequate for pyroshock simulation. However, bounded impact, a variation upon drop testing, can be used to simulate pyrotechnic shock. In normal drop testing, the test item is attached to the drop table, the table is released dropping a specified distance before impact. Both position and velocity of the test item change. In bounded-impact testing, the test item is attached to a fixture below the drop table. The fixture is anchored by a large seismic mass on springs (Fig. 31). The table is dropped impacting the fixture. There is little velocity change. The time history is very near the actual pyroshock time history. Also, the SRS are very similar. Bounded impact is the most repeatable test method (Fig. 32). Drop testing machines produce SRSs with 6 dB/oct slopes at low frequency; actual pyrotechnic devices, shaker tables, EDESS, bounded impact, and other high intensity shock simulators produce SRSs between 6 dB/oct and 12 dB/oct at low frequency. A further explanation is given in the analysis section of this paper [27:101-108, 28].

4. High Intensity Shock Machines

Laboratory shock testing can be accomplished by using the actual pyrotechnic device, a drop test machine, a shaker table, or a high intensity shock machine such

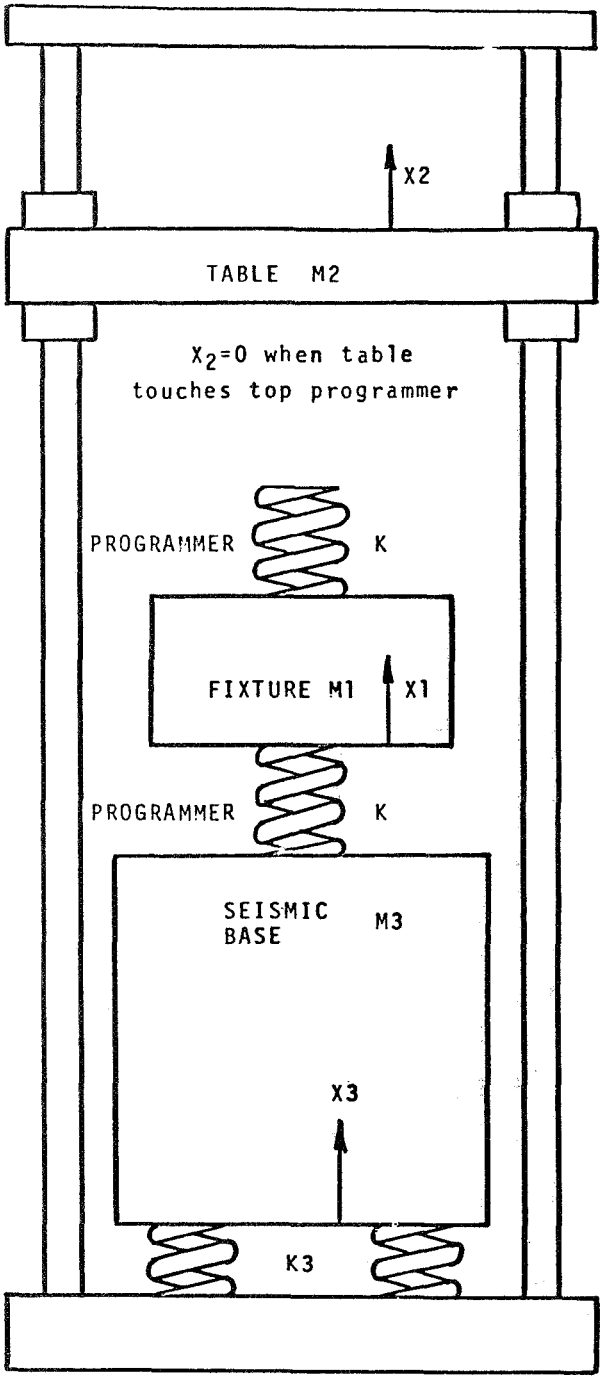

Figure 31. Standard drop machine configured for pyroshock.

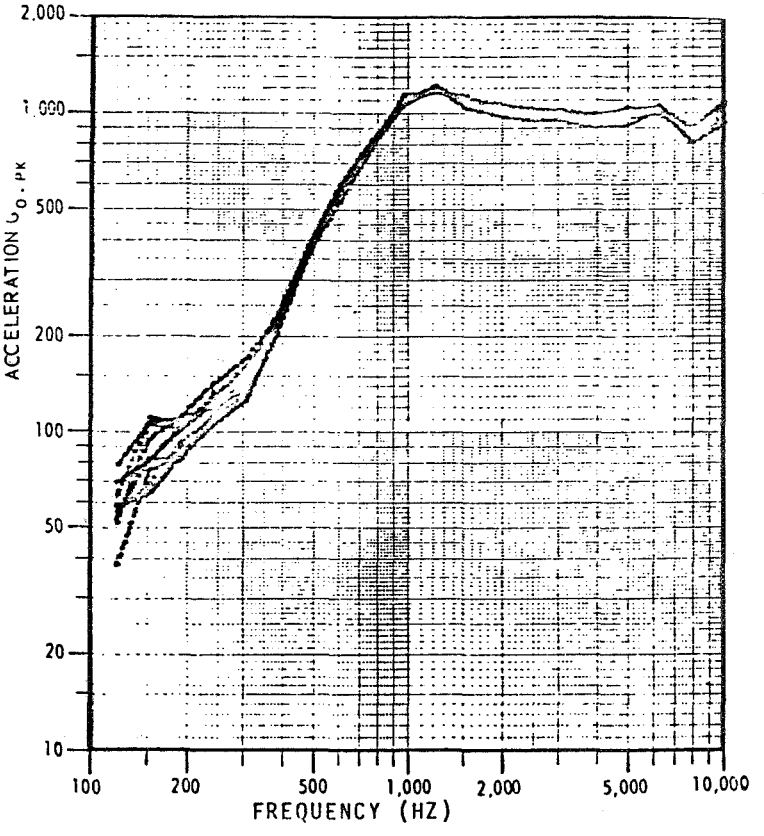

Figure 32. Repeatability of ten pyrotechnic shocks.

as the one designed by R. A. Salyer of TRW. The TRW machine consists of a test platform connected by a pair of columns to a reaction mass. Two large hydraulic jacks exert force on a piece of machined metal (machined to induce linear brittle fracture along its central portion). As the metal breaks, a shock impulse is applied to the test platform. The machine may be adjusted to provide a shock response spectrum with a minimum slope fo 6 dB/oct (velocity shock) to a maximum of 12 dB/oct (a displacement shock) [30, 35, 77].

B. Explosive Testing

1. Actual Flight

One method of explosive testing is using actual flight. "Upper Stage System Separation Test Report," SESP Flight P72-1, by E. M. Balog, gives data from flight tests [5]. "Shock Waves, How to Recognize Them, Use Them, and Provide Against Them," by C. Mas, contains shock response spectrum envelopes for various pyrotechnic devices aboard the Arianne launch vehicle. Attenuation curves for the Arianne are also included [48, 49]. Examples of flight data are in References 21, 31, 32, 33, 34, 35, 36, 89, and others.

2. Plate Testers

Another method of actual pyrotechnic testing is the pyrotechnic plate. The pyrotechnic plate simulates a pyrotechnic induced vibration environment for testing missile and space vehicle hardware. Usually, the test facility consists of a rectangular steel plate suspended from bungee cords. One or two flexible linear shaped charges are attached on the vertical edges of the plate. The test specimen is attached at the center of the plate. Current research is aimed at correlating explosive charge, wave propagation through the plate, and shock spectra accelerations at several locations on the plate. Acceleration histories, acceleration and shock spectra, and other test data are given special attention. Results tend to indicate that the shaping of the response spectrum to meet new specifications requires careful consideration to details of the linear charge. These details produce a tension wave that controls the acceleration levels at high frequency [42].

In another method of plate testing, test items are mounted on a 4 ft by 8 ft flat metal plate which is in turn driven by a flexible LSC. The charge has a separation plate sandwiched between it and the test plate. Detonation cuts the separation plate causing a shock pulse to progress through the test plate. Sample test data are also given [64].

3. Barrel Testers

To conduct shock tests using the actual pyrotechnic device, one may use the actual flight, use the actual flight structure in a ground test, or use a barrel tester. The barrel tester (Fig. 33) is a cylindrical ring and stringer structure covered with skin panels. A circumferential explosive joint, such as a LSC, cuts a metal band. Components for testing are mounted on the skin panels along with data recording devices such as accelerometers. The barrel tester gives accurate data only if it is similar in structure to the actual flight structure [79:2-39 to 2-57].

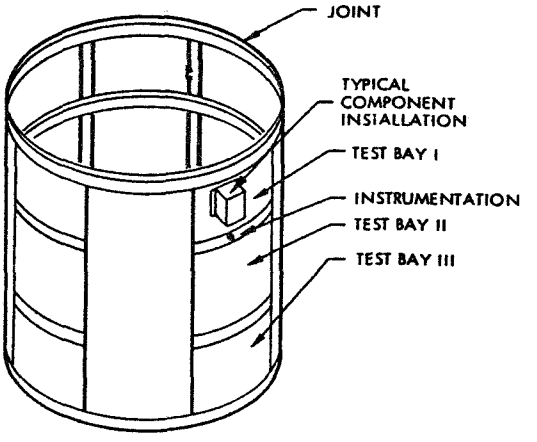

Figure 33. Barrel tester.

4. Ground Test of Flight Hardware

Detonation tests have been conducted to determine shock wave propagation velocities within pyrotechnic devices. These tests included detonating pyrotechnic compositions in sealed steel pipes and measuring propagation velocities with probes [62].

Ground tests of flight hardware use the space structure and its pyrotechnic device. "SRB Frustum/Forward Skirt Separation Tests Shock Data," is an unpublished tabloid of time histories and SRSs from ground tests [87]. Keegan and Bangs [37:131-148] also investigated ground test to determine effects of various parameters upon spacecraft separation shock.

Unpublished test reports from the two mission and eight mission certification tests of the SRB integrated receiver decoder and the six mission certification tests of the Labarge electrical cables, as well as many others, are available from NASA and other agencies [20, 39, 92].

Viking lander pyroshock environments and testing procedures were developed from ground test data [63].

IV. DATA COLLECTION AND ANALYSIS

A. Methods of Data Collection

1. Accelerometers

The most commonly used device for collecting data is the accelerometer. Accelerometers come in a wide variety of designs and frequency ranges. Literature is available from manufacturers.

2. Stress-Strain Measuring Devices

Various stress-strain measuring devices have been used to record data. Most of these devices have seen limited success. Lasers have also been used in conjunction with plastic models. But none of the above show much promise.

B. Methods of Analysis

1. General

The propagation velocity for a compression wave in a bar is $Vc = \sqrt{E/\rho}$ where ρ = density of the material and E = Young's modulus. For steel and aluminum Vc = 200,000 in./sec [31:12-37].

When a shock wave is transmitted from a primary structure to a secondary structure, the compressional wave may be transformed into a shear wave with velocity, $Vs = \sqrt{G/\rho}$, where G = the shear modulus of the material.

Shock waves attenuate with distance, $Y - ae^{-\alpha x}$, where Y = percent of peak acceleration, a = acceleration of the wave, α = a constant (slope in $in.^{-1}$), x = distance from shock in inches.

$$f \text{ (frequency in Hz)} = Vc/2L \quad ,$$

where L = length of a rod or truss in inches.

2. Time History

Time histories consist of raw acceleration, velocity, or displacement data taken directly from transducers. Acceleration time histories are used most often.

3. Shock Response Spectrum

A shock response spectrum is obtained by applying a shock pulse to a linear, undamped, single-degree of freedom system, and then plotting the maximum response of the system as a function of the system's natural frequency [39, 53]. Unless specified, the systems are undamped.

In the early 1930's, M. S. Biot devised the idea of a shock spectrum [30:42-54]. The shock response spectrum consists of an initial or primary spectrum (peak response during pulse) and a residual spectrum (peak response after pulse during ringing).

In SRSs a constant velocity at a low frequency is represented by a velocity line (a slope of 6 dB/oct), a constant displacement at low frequency is represented by a displacement line (a slope of 12 dB/oct) and at high frequencies the peak acceleration produces an acceleration line (a slope of 0 dB/oct) (Fig. 34). Notice the pyrotechnic and the square pulses as they relate to displacement, velocity, and acceleration lines [27:101-108].

When testing and analyzing data it is very important to take multiple trials so that SRSs may be verified. Frequently, subtle equipment malfunctions will give inaccurate data. An example is Figure 35 from barrel tester data. Multiple measurements gave an accurate SRS envelope. A single suspect SRS was compared with the envelope. The comparison shows the suspect to be in error. Notice the low frequency "hump" in the suspect. This hump indicated a DC shift which many charge amplifiers exhibit when encountering a large amplitude transient [79:2-45].

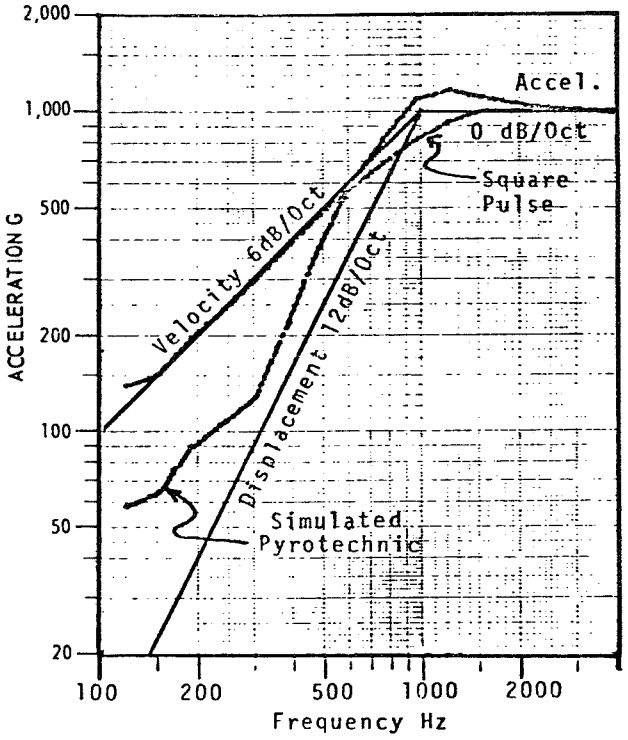

Figure 34. SRS - theoretical bounds and data.

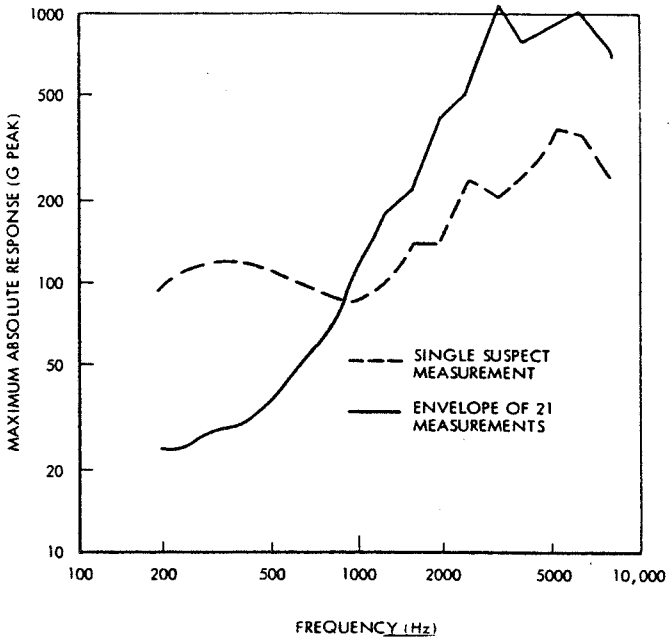

Figure 35. SRS - actual data.

Most SRSs are calculated using an impulse invariant digital simulation of a single-degree-of-freedom system. However, significant errors result in the high frequency range when the natural frequencies are greater than 1/6 of the sampling rate. The impulse invariant digital simulation can be replaced by a recursive filter with one additional filter weight. This method can be used for any natural frequency with little or no error occurring. Figures 36 and 37 illustrate SRS impulse invariant versus ramp invariant methods. Notice the error in the impulse invariant filter at high frequency [84:211-216].

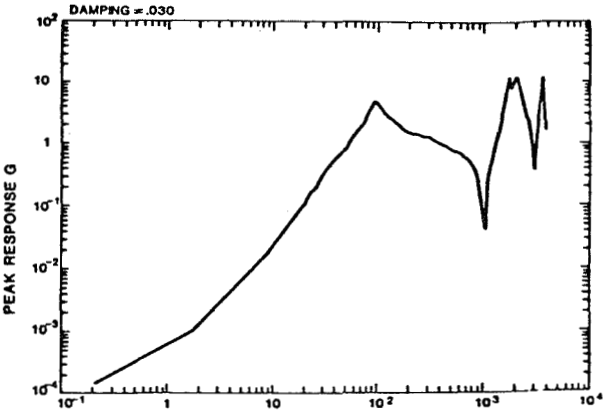

Shock Response Spectra of a 100 Hz Decaying Sinusoid Sampled at 2000 Samples/Sec Using an Impulse Invariant Filter

Figure 36. SRS - data.

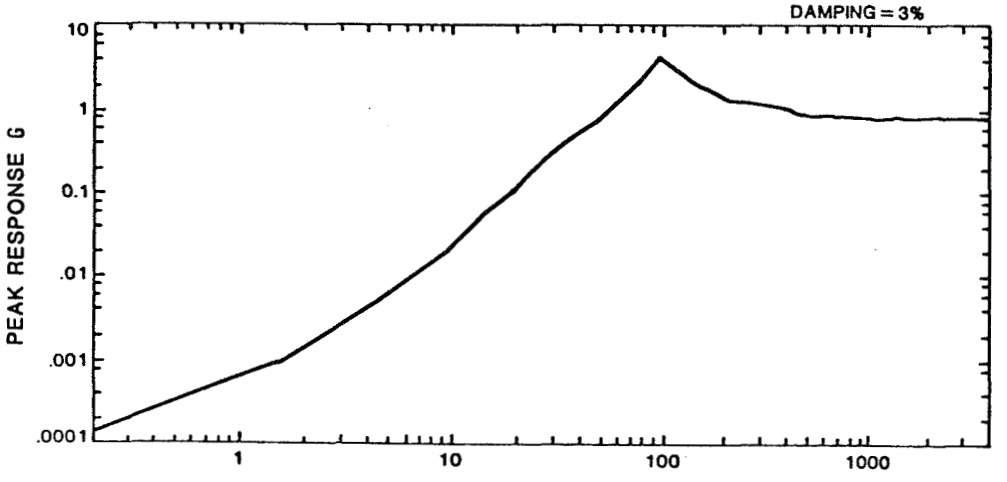

Shock Response Spectra of a 100 Hz Decaying Sinusoid Sampled at 2000 Samples/Sec Using a Ramp Invariant Filter

Figure 37. SRS - data.

LSCs produce the most severe shock source of all spacecraft pyrotechnic devices. The shock environment produced by a LSC is dependent upon the thickness of the material to be cut and the size (amount) of the explosive charge. The shock near the source is characterized by a high amplitude, high frequency acceleration time history (Fig. 38). Figure 39 illustrates the SRS for the pulse in Figure 38. As the shock moves through the structure, it is attenuated and modified by reflections and structural resonances. The time history and SRS for the same shock away from the source are illustrated in Figures 40 and 41. Figure 42 gives a comparison of shock spectra at various propagation distances [71:1-2].

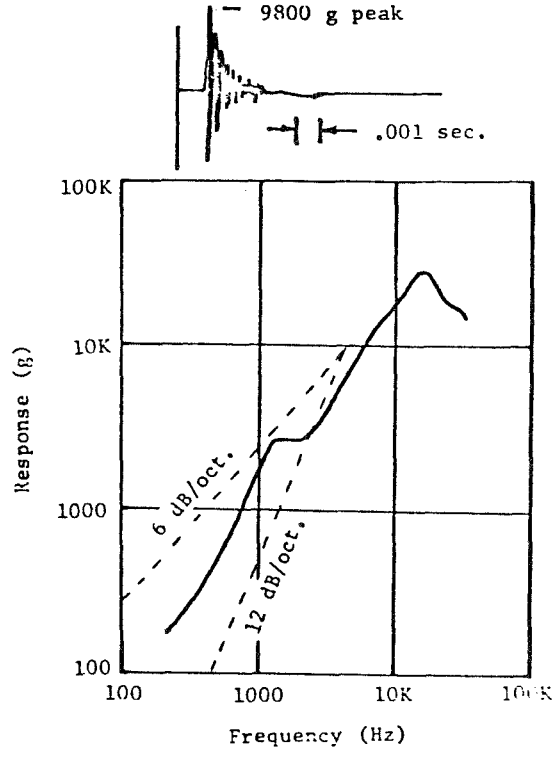

Figures 38 and 39. Acceleration time history and SRS.

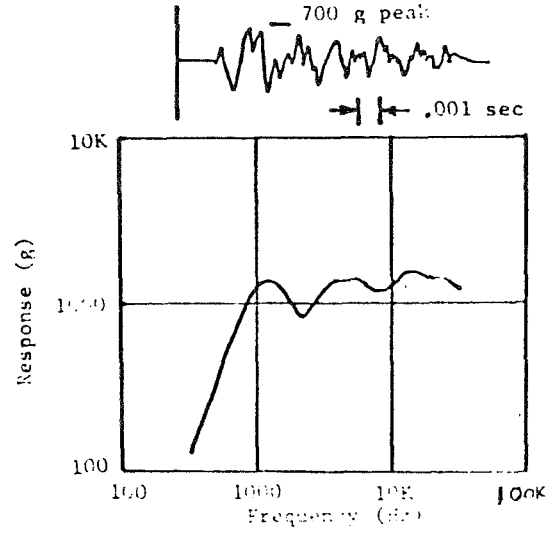

Figures 40 and 41. Acceleration time history and SRS.

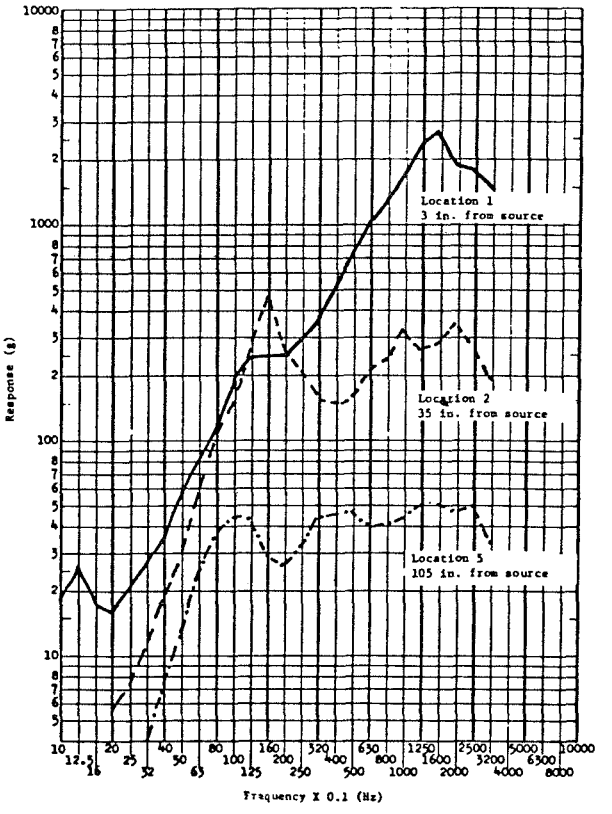

Figure 42. Comparison of SRS at various propagation distances.

Band	f(Hz)	Shock Spectrum Amplitude	Per Cent Error
Peak	1800	1678	0
2%	1820	1675	0.2
5%	1850	1657	1.3
10% (1/6 oct.)	1900	1606	4.3
20% (1/3 oct.)	2000	1425	15.1

Figure 43. Effect of frequency increment on shock spectrum amplitude.

If the frequency of the input wave falls between the natural frequencies of the analyzer oscillators, an SRS error may occur. SRS analyses are usually performed on 1/3 or 1/6 octave bands. Figure 43 shows the effect of frequency increments on SRS amplitudes. A 15 percent error is usually acceptable.

Equipment structural design, individual parts sensitivity, the test method used, and the pyrotechnic shock spectrum all affect the total equipment sensitivity to pyrotechnic shock [44].

Parker and Neubert related the normal mode solution of a vibrating rod to the pyrotechnic shock problem. Analysis provided two separate series solutions to the problem. Results were then compared with actual data [61].

Two separate facilities generated discrepant pyroshock data while testing Mariner Jupiter/Saturn spacecraft hardware. Investigation indicated that inadequate frequency response in FM tape recorders produced differing responses. Therefore, tape recorders should be chosen with very high frequency response [2].

Barrett analyzed the Viking lander capsule to develop pyroshock test requirements. Pyrotechnic sources were located, characteristics of each source were noted, and shock path distances were measured. Predictions were then made using known similar structures. The prediction was then verified by testing a full scale model [6].

Prescott collected actual pyrotechnic data from flight. He evaluated the various shock outputs in terms of shock response spectra, as to environmental shock severity. Then the analysis results were used to help redesign the pyrotechnic devices so that shock could be reduced [66].

Generating a shock spectrum in a laboratory that is identical to one from space flight may not give a satisfactory test since for each shock response spectrum there are an infinite number of pulses that can generate that spectrum. That is, the SRS is not unique [65].

A mathematical analysis is used to establish a rationale for using decaying oscillatory excitation to simulate pyroshock. Matrix algebra is used to define input pulses for an electromagnetic shaker [57].

Any complex shock spectrum can be reduced to an equivalent velocity shock spectrum. $A = VW$, where A = acceleration in ft/sec^2, V = equivalent shock velocity in ft/sec, and W = frequency in radians/sec. When plotted on log-log coordinates, this is a family of 45 deg straight lines [31:16-22].

A residual shock spectrum is the spectrum of maximum values that occur after the forcing function has ceased. This usually controls the low frequency or velocity shock region of the spectrum. The undamped residual shock spectrum (dr) magnitude is proportional to the Fourier spectrum [F(W)] magnitude and is given by $W_N dr = F(W)$. Also, $B = f_N/Q$, where B = bandwidth, f_N = natural frequency of oscillator, and Q = amplification factor.

Shock spectra have peaks at the same frequencies as do the Fourier spectra; but shock spectra are smoother and tend to average the peaks over a wide range. Shock spectra give better low frequency definition because the Fourier spectra is smoother over a larger bandwidth for typical pyrotechnic shock transients, the shock spectra provide the same frequency information as do the Fourier spectra.

In 1977 two separate facilities generated discrepant pyrotechnic shock data while testing Mariner Jupiter/Saturn spacecraft hardware. A survey of testing facilities and procedures discovered the only difference was in the FM tape recorders used to record data. One facility used a 60 in./sec recorder with a 20K Hz frequency response; the other used a 120 in./sec recorder with an 80K Hz frequency response [3:3-47; 1:11-18].

Research to determine the cause of discrepancies was warranted. A pneumatic shock simulator, which produced a shock input similar to the actual pyrotechnic event was used. The two FM recorders were used to record data from the test setup in Figure 44.

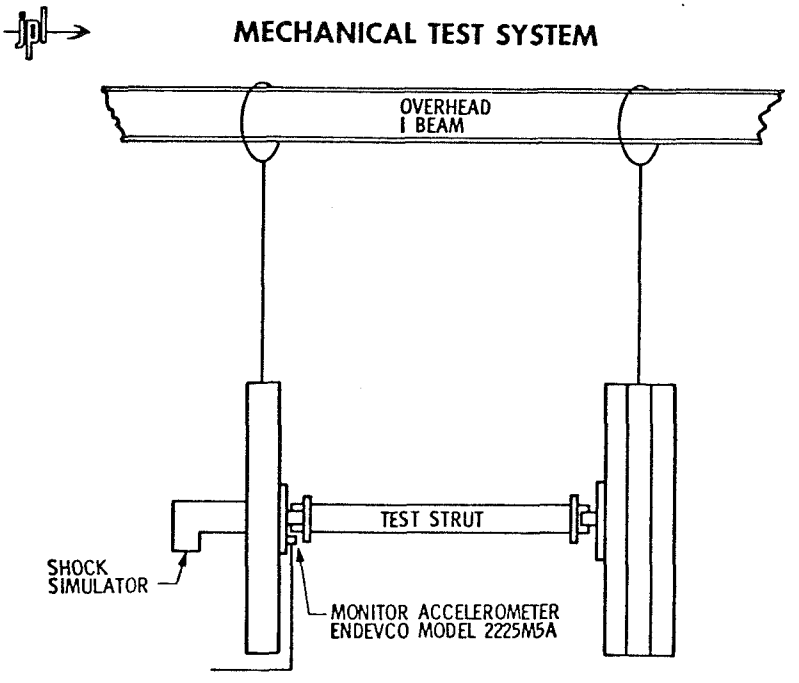

Figure 44. Mechanical test system.

The instrumentation system used is shown in Figure 45. Shock time histories were recorded on both tape recorders. Shock response spectrums were generated with a damping coefficient of 0.025 percent for Q = 20, using a digital analyzer. The SRS should be the same if no modification occurred in the tape recorders [3:3-49].

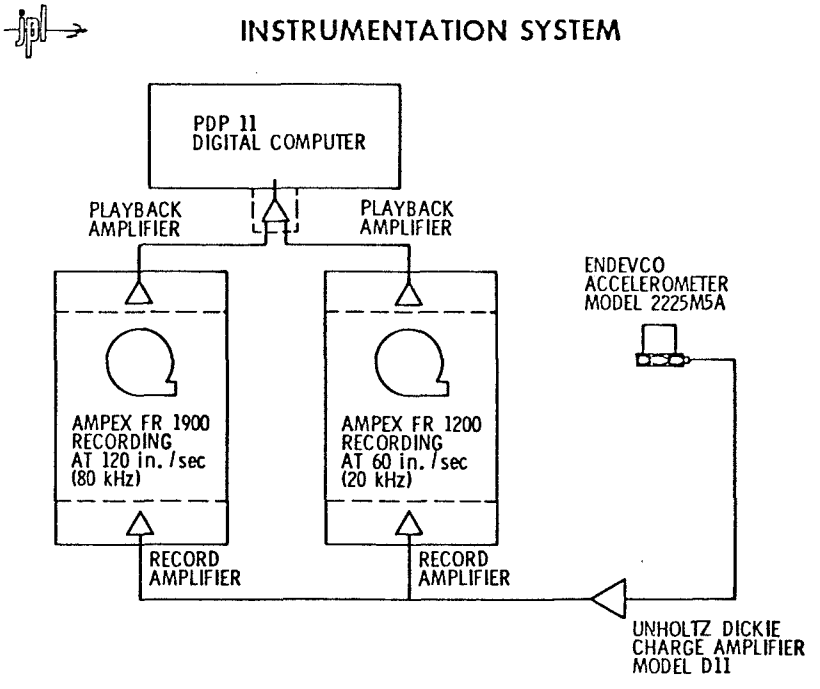

Figure 45. Instrumentation system.

However, the SRSs were different. The 20K Hz recorder was found to be clipping the peak response of the signal, whereas, the 80K Hz recorder was not. Therefore, the following conclusions were reached:

1) Before generating SRS plots from any recorded pyrotechnic event, review all instrumentation and analysis systems.

2) Use a tape recorder with high frequency response to prevent signal clipping.

3) The greater the sampling rate, the better the resolution of the data [3:3-67; 1:11-18].

Mos discusses shock waves, how to measure and define shock spectra, and how to use this knowledge to guard against damage by shock waves [14:337].

Introducing abrupt loads to a structure by explosive shock is not unique. Figure 46 compares the response of complex missile structures to four varieties of intense shock. Notice the SRSs are very much alike [74:22-27].

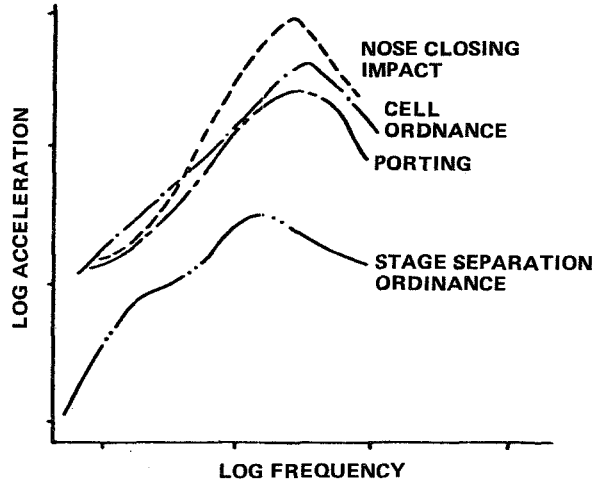

Figure 46. Four shock spectra comparing effects of various sources.

There are three means of analyzing and presenting data: The time history, the SRS, and the Fourier spectrum. Figure 47 shows these three analytical methods for the same missile structures.

The time history is a decaying transient oscillation, even though the external load was a single pulse. Notice that the frequency content of the waveform is similar whether given by shock spectrum analysis or Fourier series analysis. The Fourier amplitudes are much less than the time history amplitudes, while the shock spectrum amplitudes are much greater than the time history amplitudes. The high amplitude of the SRS is due to repeated cycles of constant amplitudes in a slowly decaying transient. The responses are almost as great as that for steady state vibration resonance.

Figures 48, 49, and 50 illustrate a dynamic model used for impact testing, the stress waves produced in the impact test, and typical calculated and measured time histories.

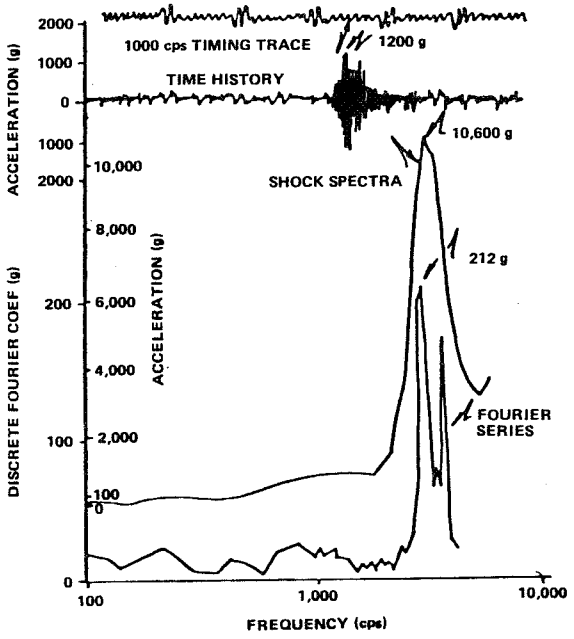

Figure 47. A comparison of three forms of data.

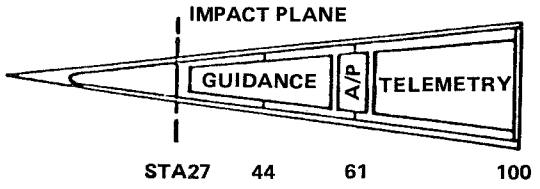

Figure 48. Dynamic model for longitudinal impact.

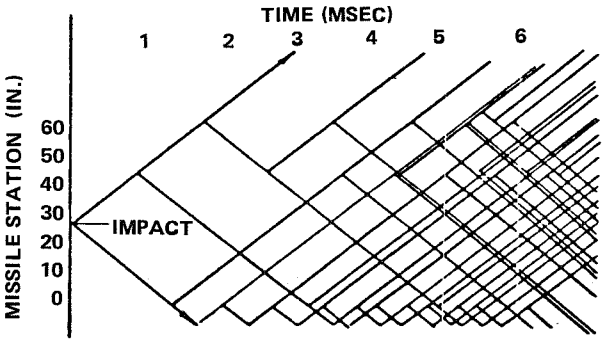

Figure 49. Transmitted and reflected stress waves.

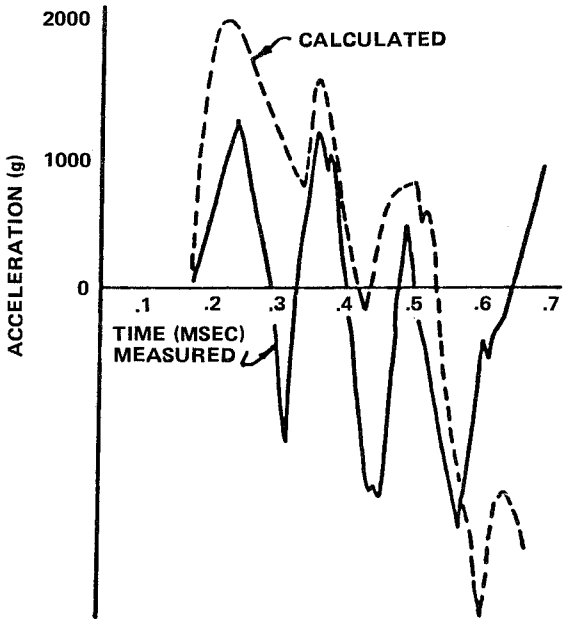

Figure 50. Calculated and measured time histories.

Figure 51 indicates the simple dynamic impact of the model. When a simple dynamic system impacts a boundary, a straight line shock spectrum results where a = VW, where a = acceleration, V = velocity, and W = frequency (Fig. 52). Figure 53 illustrates the shock spectrum (in arithmetic and log scale) for the test model.

The 45 deg slope on the logarithmic scale indicates a constant velocity portion of the spectrum. Velocity, the only variable describing the input, defines the event. Velocity also describes the stress and strain within the model by the following equations: $e = V/c$, $\sigma = \rho cV$, where e = strain, V = velocity, C = speed of sound in the material, σ = stress, and ρ = material mass density [74:22-27].

In the Mitron report, SRS and Fourier spectrums are compared. Fourier phase spectrums are illustrated [56].

The SRS and the Fourier spectrums complement each other in measuring and defining shock. The shock spectrum is more widely utilized because it gives the designer a concise indication of the maximum dynamic loads the equipment will experience (as a function of frequency) to aid in estimating damage potential [30:42-54].

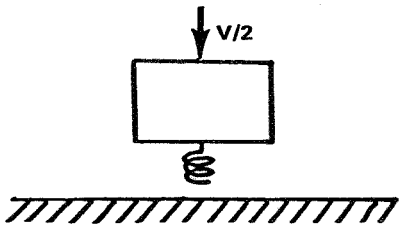

Figure 51. Simple dynamic impact.

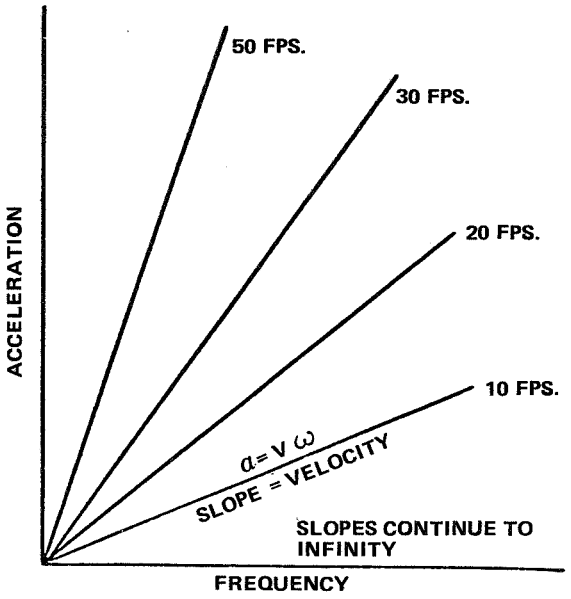

Figure 52. Shock spectra from simple dynamic impact.

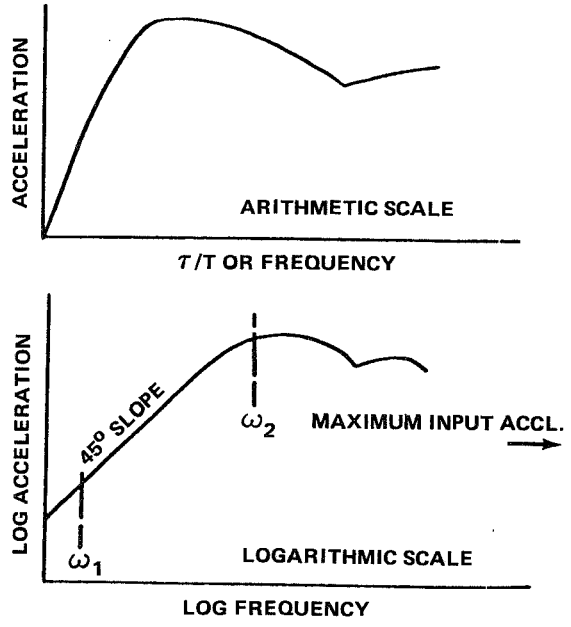

Figure 53. Two forms of shock spectra.

4. Fourier Spectrum

The Fourier spectrum gives test engineers a very sensitive technique for insuring repeatability in shock testing. The mathematician Fourier showed that any realizable transient consists of an infinite number of sine waves. The Fourier analysis consists of a Fourier amplitude spectrum (amplitude versus frequency) and a Fourier phase spectrum (phase versus frequency) [30:42-54].

The Fourier spectrum analyzes the shock pulse while the SRS determines peak response due to the pulse. The original time history can be reconstructed from the Fourier spectrum but not from the SRS. From the time history one can obtain pulse height, pulse duration, and pulse shape. Further analysis from the time history yields the Fourier spectrum (an examination of the frequency content of the time history) and the shock response spectrum (peak response value due to the frequency content of the time history) [38].

Current literature indicates that very few applications of Fourier transform techniques have been made. Efficient, accurate, and economical methods of producing Fourier transforms of complex digital records have yet to be developed [31:75-135]. Figure 54 compares SRS and Fourier spectra for a shock impulse.

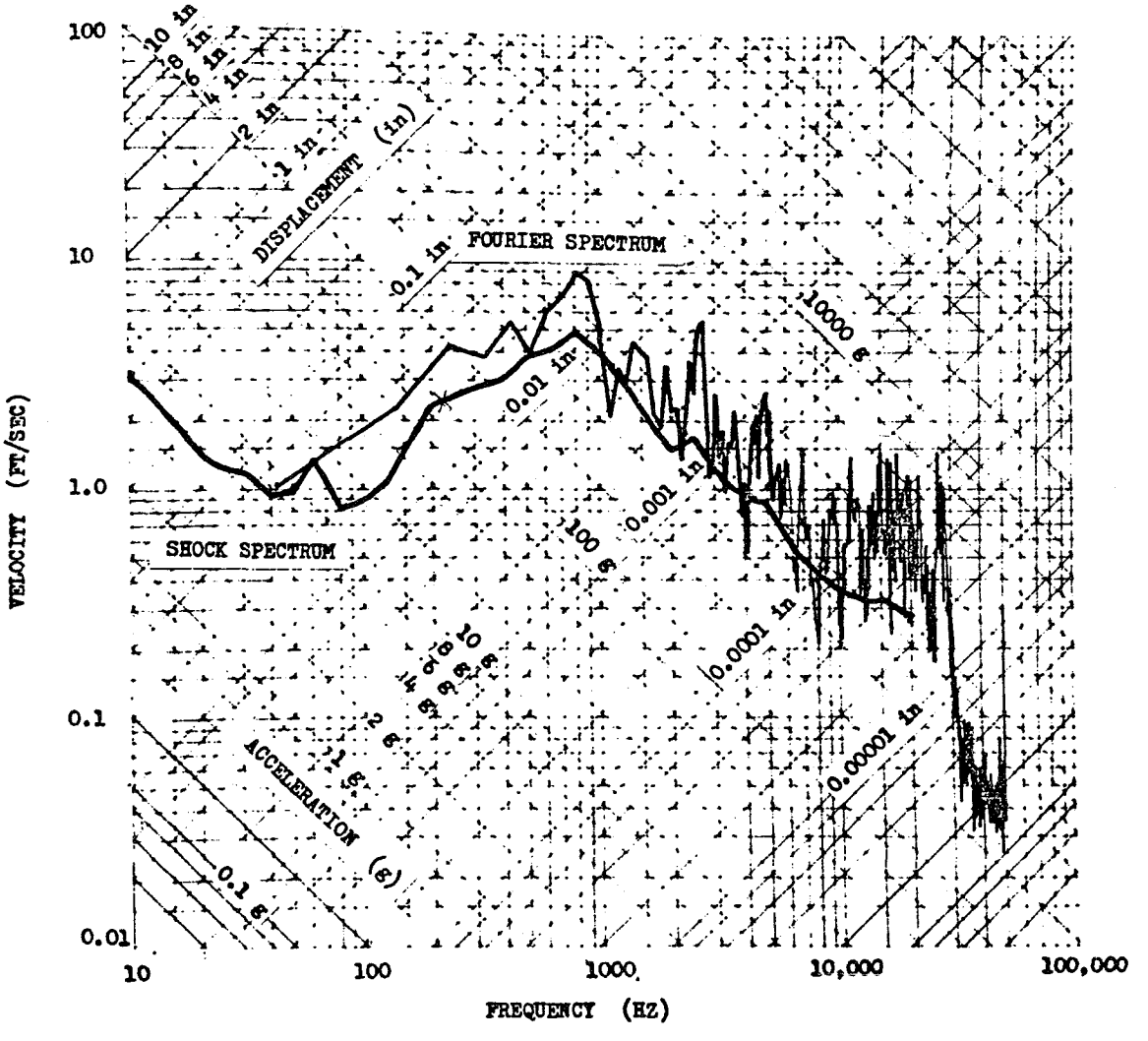

Figure 54. Fourier spectrum - SRS plots.

5. Acceleration from Strain Measurement

At present, the state-of-the-art is that pyrotechnic shock could not be predicted. The only approach to evaluate equipment is to proof test. The most severe loading condition appears to be the separation of two rocket stages by using primacord to tear a circumferential V-band joint. Primacord is a linear non-shaped charge. From a design viewpoint a force-time output would be more useful than an acceleration spectrum because force-time loading could be used as design loading [59:6].

Experiments have shown that because of the shortness of the pulse compared to the diameter of the bar, dispersion of the wave occurs. Therefore, radial inertia effects need to be included as in the Love Bar Theory. The same experiments indicated that the strain pulse length 10 in. from the explosion is only 12 microseconds. The associated acceleration at 12 microseconds is 80,000 Hz. In other words, near source measurements at 20,000 Hz or less are inadequate with respect to high frequency shock.

Primacord with 4 gr/ft of explosive was used for the experiment. The charge was detonated using electrical blasting caps. The detonation velocity was 21,000 ft/sec. Detonation of 2 in. of primacord takes about 10 microseconds. The primacord is attached to brass plates to simulate the tearing of metal in a V-band joint. Foil, resistant-type strain gages were used along with 100,000 Hz bridge amplifiers and an 80,000 Hz tape recorder. Signals were recorded at 120 in./sec. Strain gages were located 5, 10, 20, and 50 in. from the end of the bar (source). The strain signals should be of the same magnitude and phase for axial pulses. Pure bending signals would be of the same magnitude but 180 deg out of phase (Figs. 55 and 56). A primarily compressive pulse first occurs at t_1. It is reflected as a tensile pulse at t_2 after traveling 160 in. It then returns as a compressive pulse at t_3 after traveling 40 more inches. Wave velocity calculated between pulses is 210,000 in./sec; near the expected elastic wave speed for steel [59:6].

The elastic bar equation is as follows:

$$E \frac{\partial^2 U}{\partial X^2} = \rho \frac{\partial^2 U}{\partial t^2}$$

and the Love equation is as follows:

$$E \frac{\partial^2 U}{\partial X^2} = \rho \frac{\partial^2 U}{\partial t^2} - \rho \gamma K^2 \frac{\partial^2 \mu}{\partial X^2 \partial t^2}$$

where ρ = density, E = Young's modulus, γ = Poisson's ratio, K = radius of gyration of the cross section about a longitudinal axis.

The force-time input to the bar was as follows:

$$F(t) = Fo \sin wt \qquad 0 \leq t \leq \pi/W = to$$

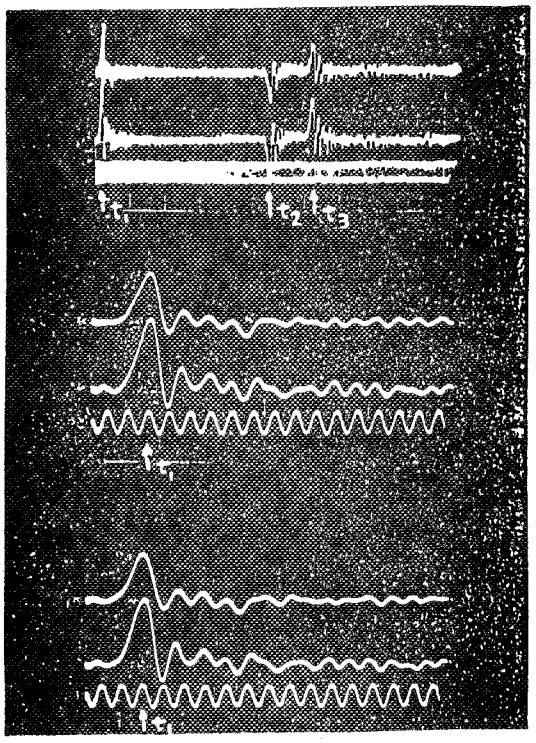

Figure 55. Time histories.

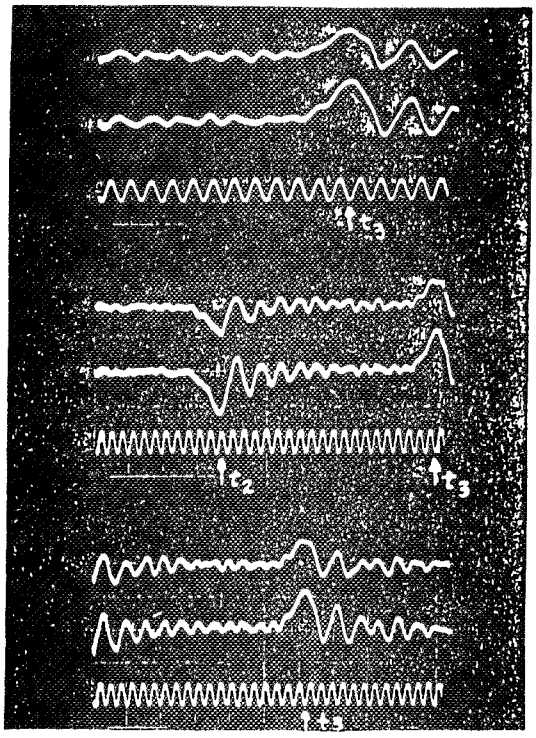

Figure 56. Time histories.

$F(t) = 0 \qquad t > \pi/W = to$

Now for $U = f(X - Ct)$, strain $= \partial U/\partial X = f'(X - Ct)$, particle velocity $= \partial U/\partial t = -Cf'(X - Ct)$, and particle acceleration $= \partial^2 U/\partial t^2 = C^2 f''(X - Ct)$. Therefore, acceleration can be related back to strain [59].

Subscale Lexan plastic models of spacecraft structures have been tested for vibration response. Structural response was measured by strain, accelerometers, and by a camera (photoelasticity was measured using fringe patterns produced by the Lexan). Results were very similar for all three measuring methods. This model method can be used to obtain reliable data [89].

V. METHODS OF REDUCING SHOCK OR SHOCK EFFECTS

A. Shock Source Reduction

The shock source can be reduced by modifying the pyrotechnic device but modification is costly and time consuming. This is accomplished by experimentally determining the smallest charge and the best charge shape for performing the desired cutting task. A better method is source isolation [7:21-32, 36:21-22].

B. Shock Source Isolation

Shock may be reduced by isolating sources. A small amount of isolation may be accomplished by increasing LSC standoff. The best method of isolation is using a bellows assembly. Expansion bellows are an expandable tube containing a LSC. The structure to be cut is severed by the bellows which shears rivets by expanding when the LSC detonates [7:21-32, 31:75, 36:21-22]. In most cases, isolation of shock sources is costly and time consuming also. The three less costly and less time consuming methods of shock reduction are shock attenuation methods, shock mounting, and component redesign or modification.

C. Increase Attenuation of Shocks

When shock pulses cross mechanical joints, attenuation occurs due to reflections of the shock wave. When two or more materials make up the joint, attenuation is increased [7:21-32]. Joint attenuation tests were conducted using the test setup in Figure 57. A shock pulse was applied on one side of the joint but the shock level was measured on both sides. Metals, hard nonmetals, and soft nonmetals were used as insert joint materials (Fig. 58).

The joint was tested without an insert to give a base comparison value. Thirty-five inserts were tested. Insert effectiveness was judged by considering shock response spectra from data measured on the joint side away from the shock with and without an insert. Figure 59 lists joint insert material and thickness. Figure 60 gives percent shock reduction.

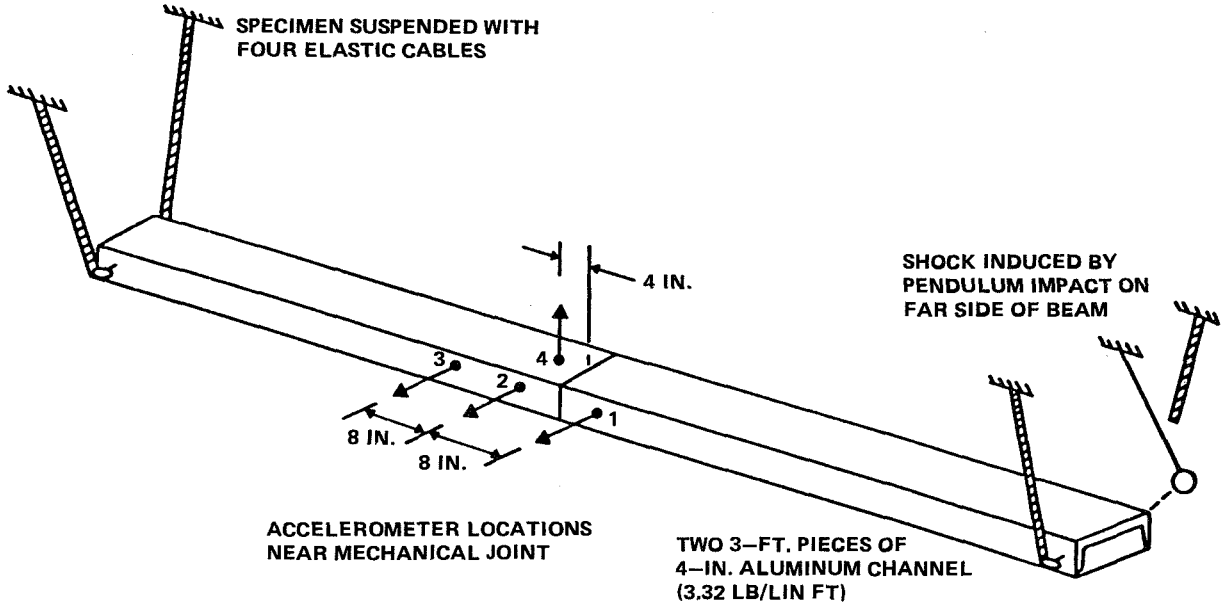

Figure 57. Test apparatus.

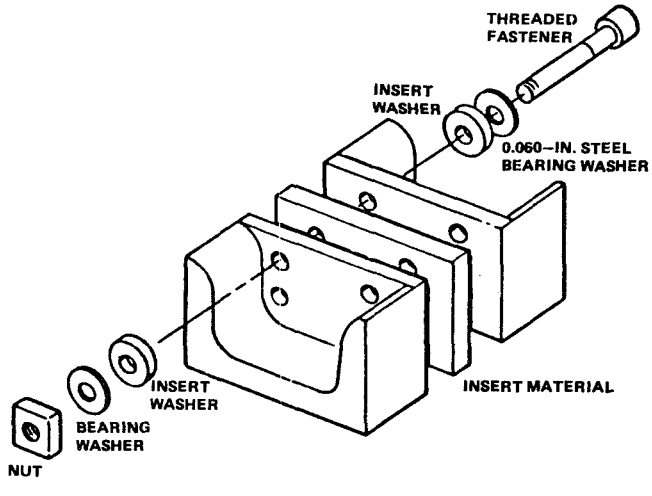

Figure 58. Joint configuration.

JOINT CONFIGURATION NUMBER	INSERT MATERIALS	INSERT WASHERS USED	INSERT THICKNESS (IN.)	DUROMETER (SHORE A)
1*	NONE	NO	—	—
2	STEEL (S)	NO	0.060	—
3	MAGNESIUM (M)	YES	0.125	—
4	TEFLON (T)	YES	0.125	—
5	PHENOLIC	YES	0.100	—
6	FIBERGLASS	YES	0.125	—
7	ASBESTOS	YES	0.125	—
8	S–S	NO	+	—
9	T–M–S–T	NO	+	—
10	M–S	NO	+	—
11	M–S–M–S	NO	+	—
12	S–M–S	NO	+	—
13	M–S–M	NO	+	—
14	M–S–S–M	NO	+	—
15	1 STEEL WASHER (W)	NO	0.060	—
16	2W	NO	+	—
17	4W	NO	+	—
18 §	4W	NO	+	—
19	6W	NO	+	—
20 q	6W	NO	+	—
21 q	M–S–S–M	NO	+	—
22 *	NONE	NO	—	—
23 q	NEOPRENE	YES	0.063	50
24 q	NEOPRENE	YES	0.063	60
25 q	SILICON RUBBER	YES	0.063	50
26 q	VITON A	YES	0.063	75
27 q	ADIPRENE	YES	0.060	87
28 q	VITON A	YES	0.125	75
29 q	NEOPRENE	YES	0.250	80
30 q	VITON A	YES	0.094	75
31 q	NEOPRENE	YES	0.125	50
32 q	NEOPRENE	YES	0.250	50
33 q	ALUMINUM	YES	0.250	—
34 q	ALUMINUM	NO	0.250	—
35 q	LEAD	YES	0.100	—

* HARD JOINT (BASELINE) CONFIGURATIONS.
\+ THICKNESS OF MULTIPLE INSERTS IS THE SUM OF INDIVIDUAL THICKNESSES PREVIOUSLY LISTED.
§ LOOSE JOINT.
q RUBBER SLEEVES AROUND BOLTS.

Figure 59. Insert materials table.

Joint Configuration Number	Shock Reduction (Relative to Hard Mount) at Spectrum Peaks (%)		
	Location 2	Location 3	Location 4
2	16		22
3	20		14
4	40		25
5	4		11
6	12		14
7	16		14
8	32		31
9	20		20
10	36		51
11	40		34
12	34		40
13	40		17
14	32		40
15	24		34
16	0		6
17	0		14
18	46		48
19	16		20
20	56		62
21	40		40
23	0	21	
24	0	0	
25	47	42	
26	14	15	
27	23	42	
28	35	50	
29	23	47	
30	42	42	
31	44	52	
32	41	40	
33	17	15	
34	17	0	
35	35	40	

Figure 60. Shock reduction table.

Figures 61 through 66 show SRS data for various joint inserts.

From joint attenuation tests, the following general observations were made:

1) Mechanical joints without inserts provide about a 50 percent reduction in SRS at all frequencies.

2) A heat-shrink rubber sleeve around fastening bolts reduces shock significantly.

3) Loosely assembled joints reduce shock across the joint.

For metal inserts:

1) Lead was the only metal to significantly reduce shock when used alone.

2) Multiple inserts of steel are no more effective in shock reduction than are solid steel inserts. Both give only slight reduction.

3) Alternate layers of steel and magnesium give the greatest reduction, 30 to 40 percent.

4) Reduction of shock by using inserts is effective only in the upper frequency range. There is no reduction below 1500 Hz.

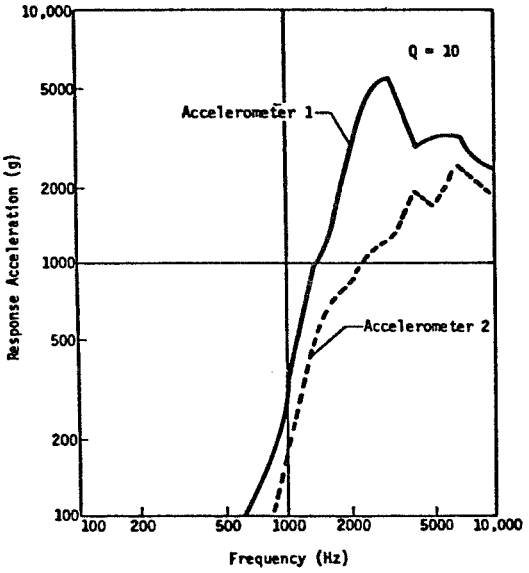

Figure 61. SRS data.

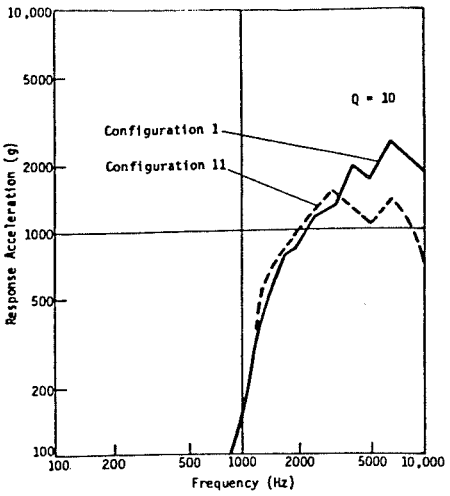

Figure 62. SRS data.

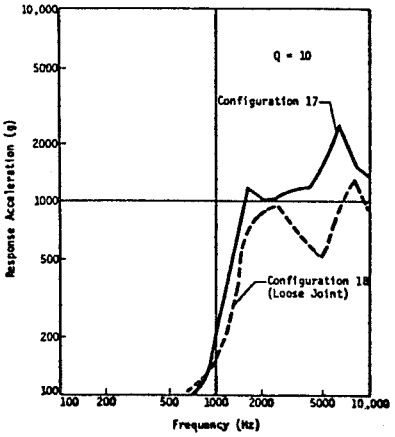

Figure 63. SRS data.

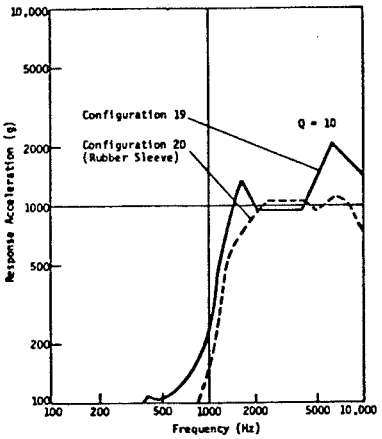

Figure 64. SRS data.

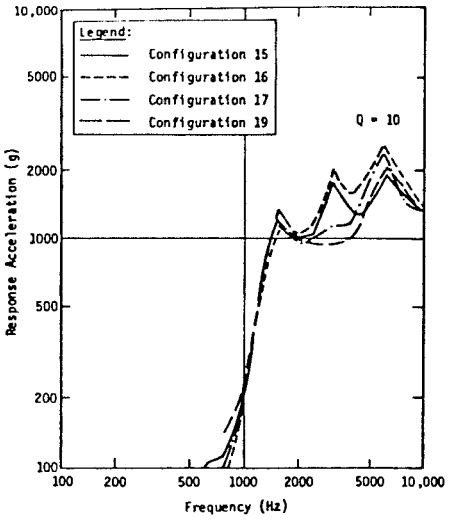

Figure 65. SRS data.

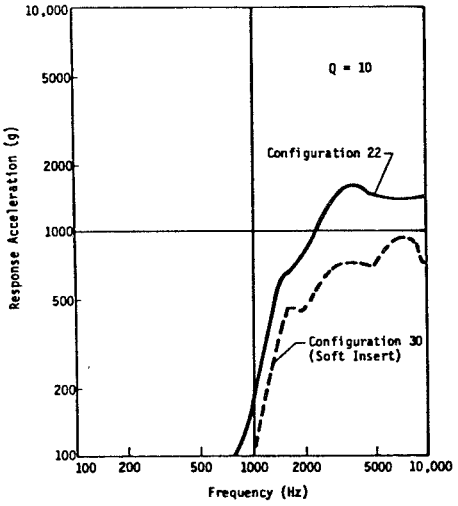

Figure 66. SRS data.

For hard nonmetals: No significant attenuation occurred using hard nonmetals.

For soft nonmetals: About 40 percent shock reduction was demonstrated at high frequencies with 30 percent at lower frequencies.

D. Use Shock Mounts

There are several ways to shock mount sensitive components:

1) Hard Mounts: where the impedance mismatch of different materials reduces shock.

2) Mounting Brackets: where the impedance effects of bracket geometry reduce shock.

3) Soft Mounts: where relative motion reduces shock.

The greatest shock reduction is achieved with soft mounts. The soft mounts create a low frequency single-degree-of-freedom system that filters off high frequency shock [7:21-32].

Using a shaker table, component isolation tests were performed on 15 different component configurations. Figure 67 illustrates the component shock test setup and mount details. Figure 68 shows the input SRS for the shaker table. Figure 69 gives the type and thickness of mount material used in each configuration. Figure 70 presents percent shock reduction relative to hard mount based upon SRS comparison. Figures 71 and 72 illustrate typical SRS for the component shock mount test.

Component isolation test results indicate that shock attenuation increases as the mounted natural frequency decreases. Figure 73 attempts to analytically predict the data; the prediction was futile. As in all pyrotechnic research to date, solutions are empirical.

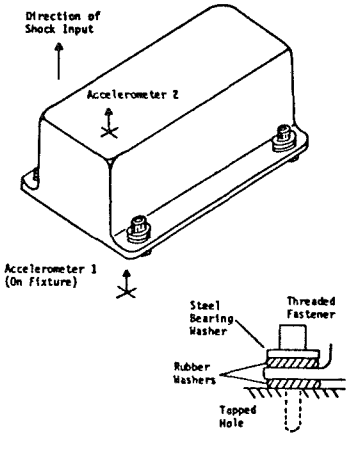

Figure 67. Test component.

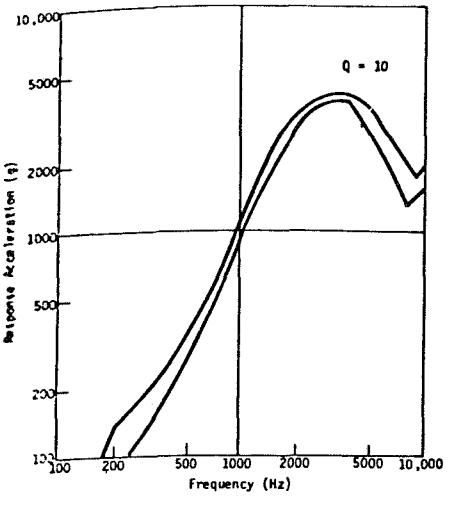

Figure 68. SRS envelope.

Component Configuration Number	Isolation Washer Description			Mounting Torque (in.-lb)
	Material	Thickness (in.)	Durometer (Shore A)	
1*	None	--	--	100
2	Viton A	0.094	75	1.5
3	Viton A	0.094	75	1.0
4	Viton A	0.125	75	1.0
5	Silicon Rubber	0.063	50	†
6	Silicon Rubber	0.063	50	1.0
7	Neoprene	0.125	50	†
8	Neoprene	0.125	50	1.0
9	Neoprene	0.063	50	†
10	Neoprene	0.250	50	1.0
11	Neoprene	0.250	50	†
12	BTR	0.125	40	†
13	BTR	0.125	40	1.0
14	Mozite	0.250	10	†

*Hard mount (baseline) configuration.
†Torque too small to measure--material flow evident.

Figure 69. Isolation washer table.

Component Configuration Number	Approximate Mounted Natural Frequency (Hz)	Shock Reduction Relative to Hard Mount (%)
2	--	0
3	700	25
4	600	33
5	375	88
6	450	84
7	450	71
8	600	41
9	550	50
10	320	75
11	225	84
12	300	90
13	360	88
14	100	94

Figure 70. Shock reduction table.

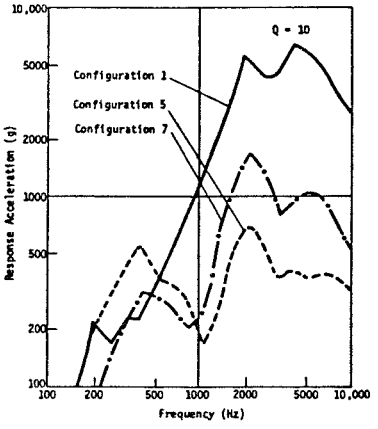

Figure 72. SRS data.

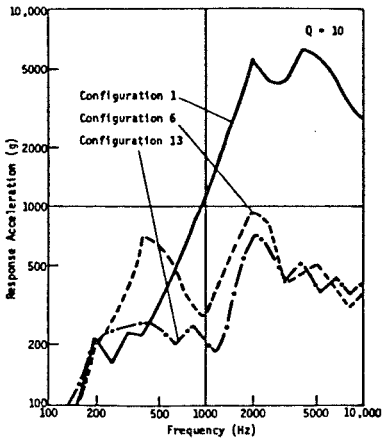

Figure 71. SRS data.

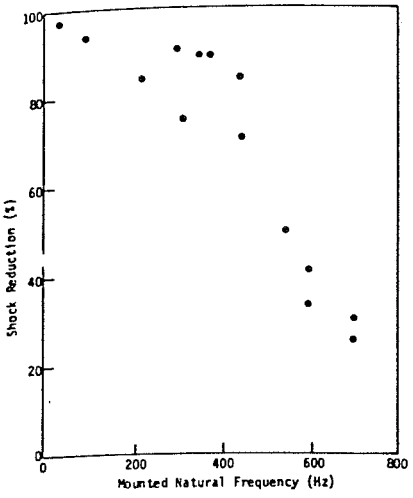

Figure 73. Shock reduction versus frequency.

E. Modify or Redesign Equipment Receiving Shock Damage

Equipment can be completely redesigned, isolating or removing a component damaged by shock in qualifying test. This can be very costly. Or equipment can be modified. Modification can be as simple as moving a component to another location. An example might be rearranging printed circuit boards in a card rack.

VI. SUMMARY OF THE "AEROSPACE SYSTEMS PYROTECHNIC SHOCK DATA" REPORT

This report is a result of a study by Martin Marietta Corporation for NASA under contract NAS5-15208 [31, 32, 33, 34, 35, 36]. The results of this study are as follows:

1) Reduced pyroshock data from many aerospace systems were compiled. A total of 2837 measurements were compiled.

2) Characteristics of pyroshock transients were defined.

3) The quality of all available pyroshock data was evaluated.

4) Measurement systems for ground test and flight were recommended.

5) Design guidelines applicable to structure and equipment design were prepared.

6) Test simulation techniques were recommended.

7) Pyrotechnic systems were classified as to their resulting shock or damage effects.

8) The effects of structural configuration and materials on resulting shock characteristics were evaluated.

9) Further research studies were formulated.

10) Shock propagation theory was applied to some cases.

11) A full scale ground test program on the Titan III structure was performed.

Volume summaries are as follows:

Volume I: Results of the study.

Volumes II and III: Compiled data from work done in the study program. Volume II contains the LSC data.

Volumes IV and V: Data and analysis submitted by Lockheed under a subcontract. Volume IV contains LSC data.

Volume VI: Design guidelines manual.

Although this report was published in 1970, it is still the most complete and accurate work of its kind. The report contains the most complete set of LSC induced pyroshock data available. Figures 74 and 75 are examples of LSC data. Volume VII is an extension of the six volume set. Volume VII was a result of contract NAS5-21242, a follow-up of NAS5-15208. Volume VII investigates the effects of mass loading upon pyroshock environment [23].

Truss structures and airframe skin and stringer structures were pyroshock tested with various weighted components mounted upon them so that shock variation as a function of mass loading could be determined. No definite relationship between mass loading and the variation in shock due to mass loading could be determined.

Articles 51, 52, 70, and 71 are papers summarizing the six volume study above.

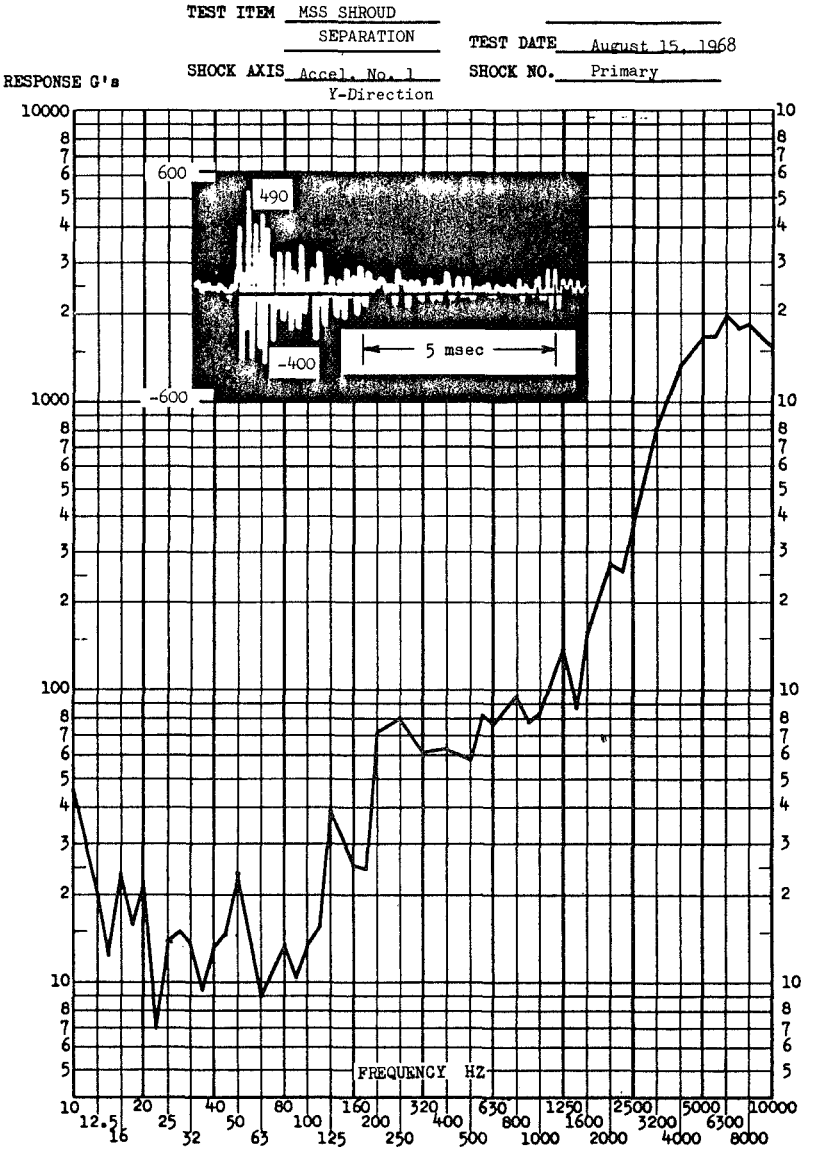

Figure 74. MSS shroud separation data.

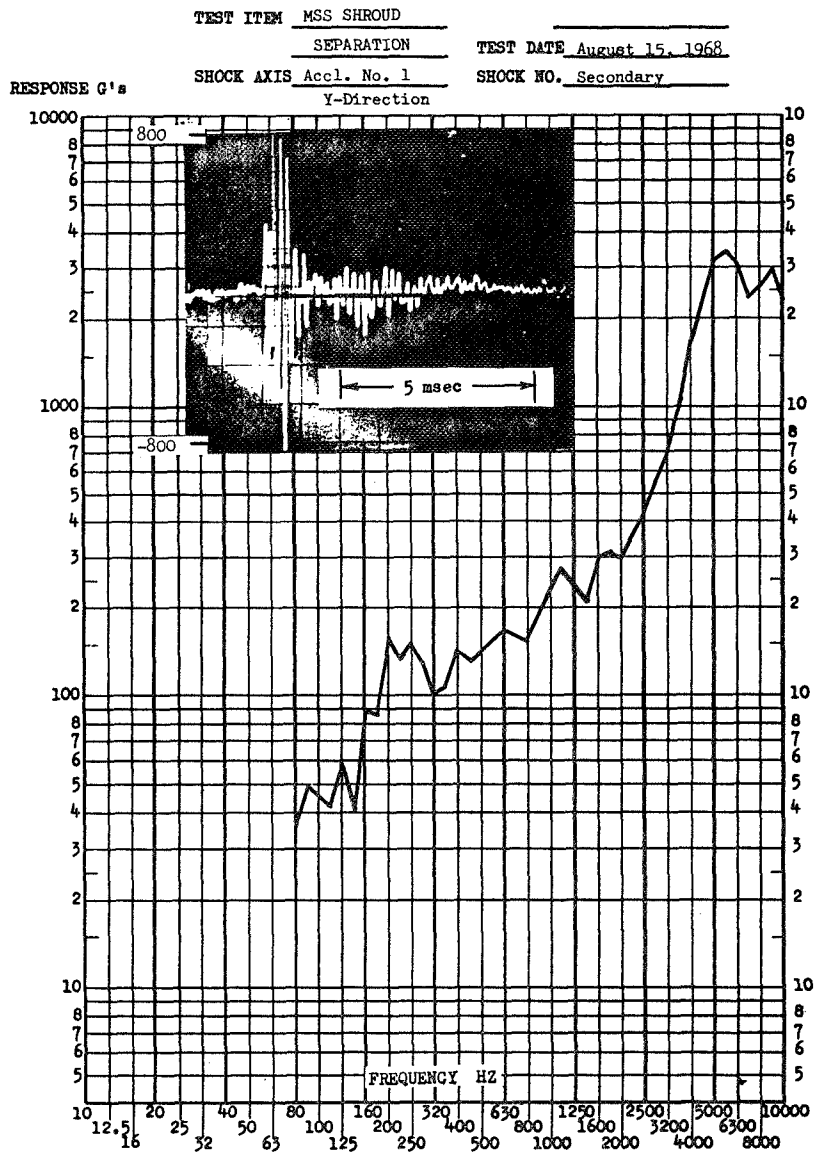

Figure 75. MSS shroud separation data.

VII. PYROTECHNIC SHOCK DESIGN CRITERIA

A. Types of Guidelines

In the design manual [36] there are predicted SRS's, attenuation curves for various structures, and attenuation values for joints.

B. Derivation of Guidelines

Attenuation guidelines are derived empirically for various structures. Shock levels are measured as a function of distance from source. Then the shock levels are plotted versus distance from source. SRS guidelines are developed by taking a

maximum value smooth curve envelope of STS data. Values of shock attenuation over various types of joints have also been measured and listed in tables. Figures 76, 77, and 78 illustrate attenuation data.

All the design curves in the design guide must be used with much discretion. These curves are empirical; they depend strongly upon the parameters used to calculate them. Major parametric variation can result in design error. The chief tool of the design engineer is the SRS (Fig. 79). Notice the test setup. The output acceleration, Y(t), is shown as a time history shock pulse. The pulse is then analyzed to yield the maximum response acceleration as a function of frequency, Ymax(f), for a single-degree-of-freedom system.

A SRS exhibits amplitude and frequency information characteristics of the time history. It is used in the aerospace industry to specify shock environments.

A shock spectrum for specifying equipment qualification levels should be calculated using full-scale test data. When this is not possible, a preliminary spectrum can be estimated from the expected level at the source using empirical attenuation curves. Figure 80 is an example of a suggested SRS.

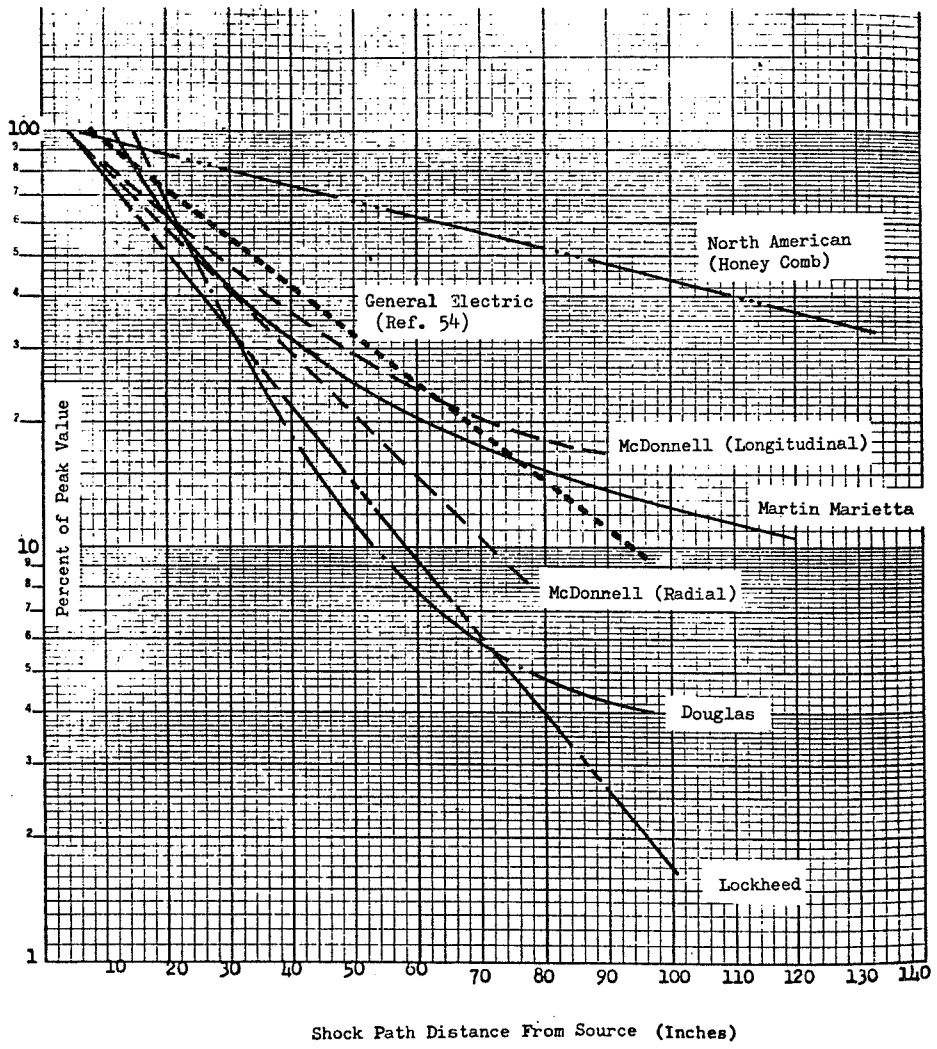

Figure 76. Attenuation versus distance from source.

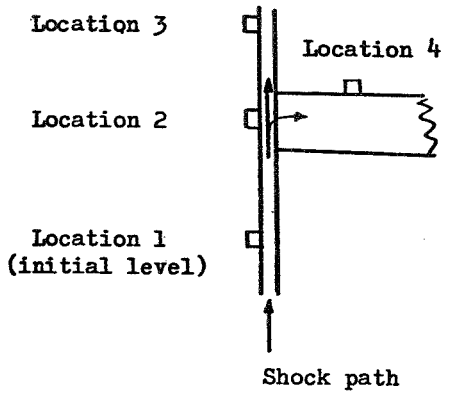

Large amount of structure disperses shock

Location	Reduction of Level
2	0%
3	75%
4	30%

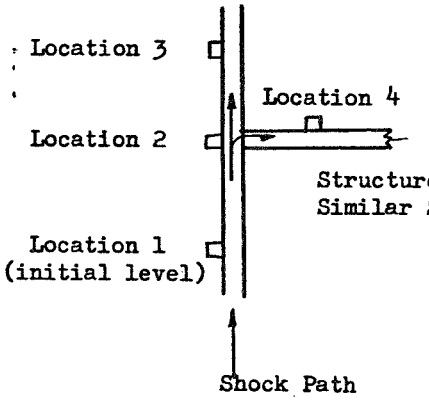

Structures of Similar Size

Location	Reduction of Level
2	0%
3	20%
4	70%

Figure 77. Attenuation for various joints.

Interface	Per Cent Reduction
Solid Joint	0
Riveted butt joint	0
Matched angle joint	30-60
Solid joint with layer of different material in joint.	0-30

Figure 78. Attenuation for various joints.

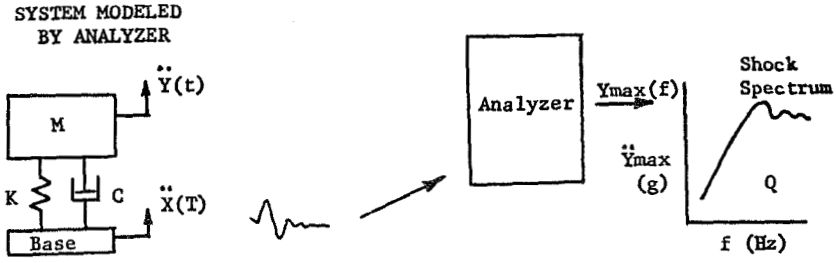

$\ddot{X}(t)$ input acceleration

$\ddot{Y}(t)$ output acceleration

K = spring constant

$C/C_c = \zeta$ ratio of actual damping to critical damping

Q = $1/2\zeta$ amplification factor

f = $\frac{1}{2\pi}\sqrt{K/M}$, natural frequency of system

M = mass

Figure 79. Data analysis methods.

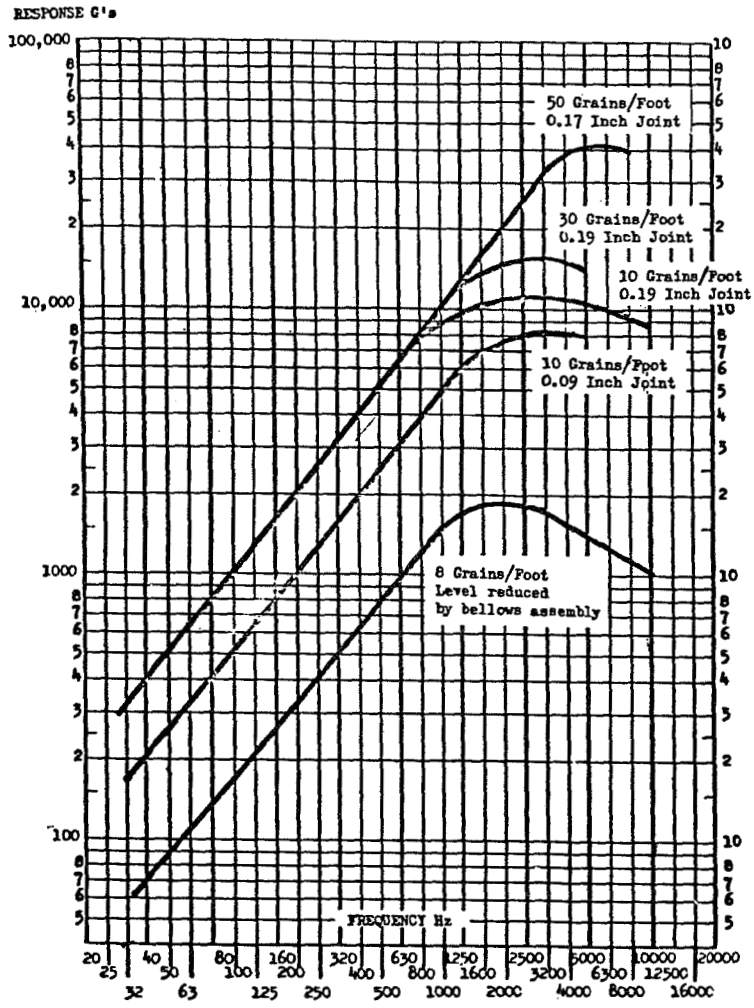

Figure 80. Predicted SRS.

C. Usage

Example Problem: Suppose a cylindrical shell 0.19 in. thick at the joint is to be cut by a 10 grain/ft LSC. A component is to be placed 40 in. from the charge. Derive a "rough estimate" SRS for the component.

First, using Figure 81, calculate the attenuation for 40 in. from the source for a cylindrical shell. Thirty percent of the source shock remains. Next, we go to Figure 82. Figure 82 is calculated for 10 in. from the source. So the attenuation factor for 10 in. from the source is needed also. Figure 81 gives 84 percent of the shock remaining for 10 in. The net percentage of the shock remaining relative to Figure 82 can be calculated by ratio: 30%/100% = X%/84% → X% = 25.2%. That is, 25.2 percent of the SRS given in Figure 81 remains. In Figure 82, find the suggested SRS for a 0.19 in. joint, 10 grains/ft charge and cut. For each frequency find the SRS value and multiply that value by 25.2 percent to get the new SRS. For example, at f = 40 Hz, a value of 400 g is given; 400 g x 0.252 = 100.8 g. Repeat that process for each frequency. Figure 82 also gives the result or calculated SRS for our component. Remember this SRS is only a "ball park" estimate. If overdesigning cannot be tolerated, actual testing must be done to give more accurate results.

It should be noted that as a shock moves away from a source, the high frequency acceleration attenuates much more rapidly than the low frequency. Therefore, the SRS of our example is high in the high frequency range. However, as a design envelope this is perfectly acceptable.

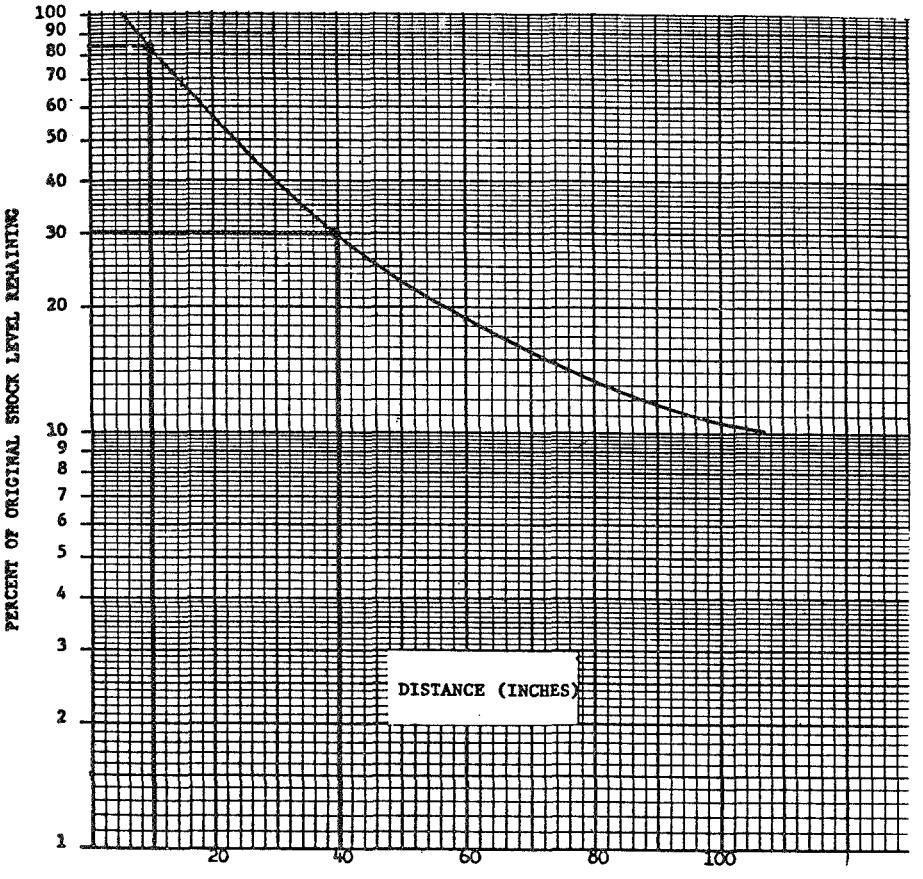

Figure 81. Attenuation for cylindrical shell.

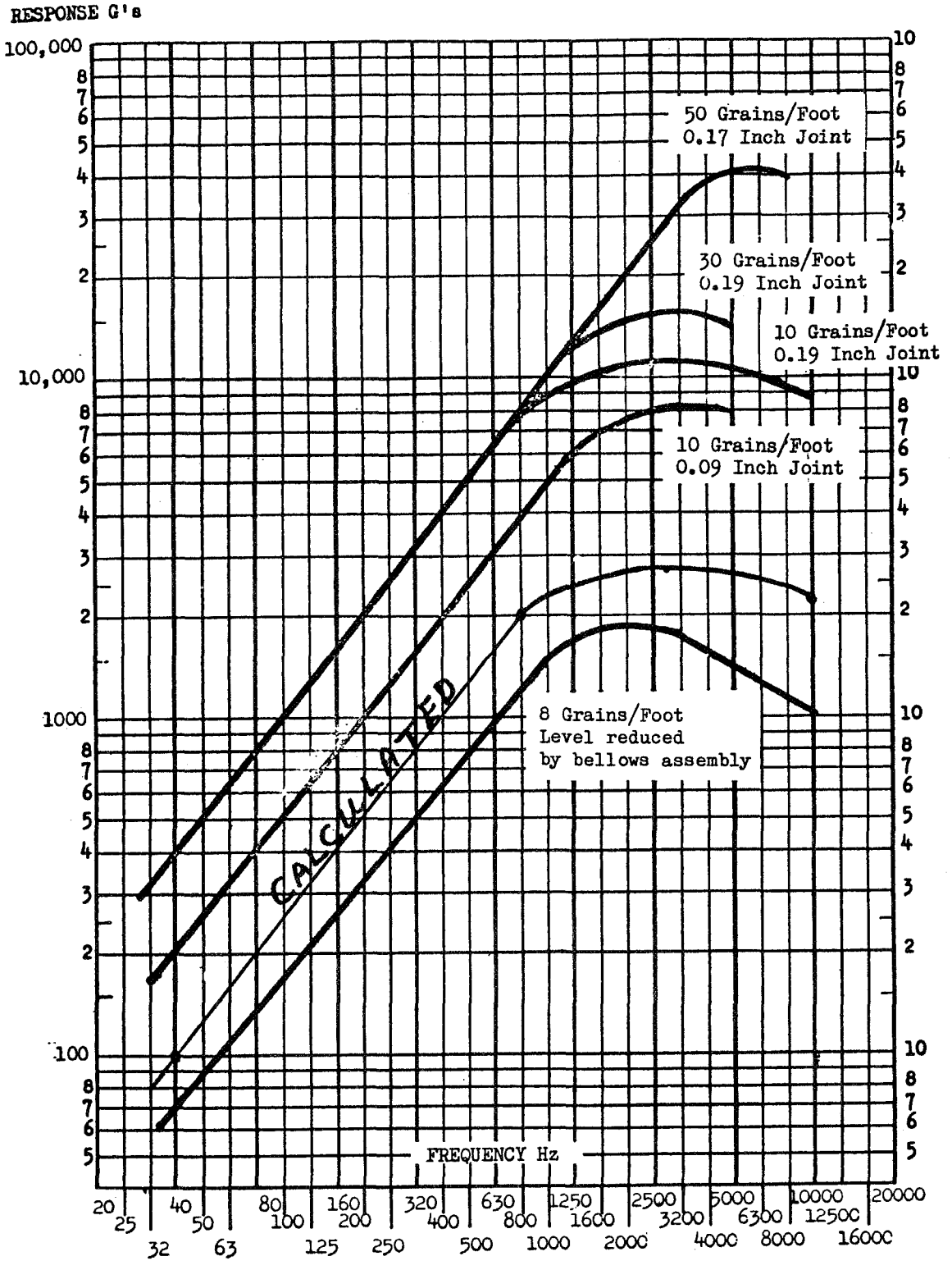

Figure 82. Predicted SRS.

VIII. SUMMARY

Linear shaped charges use the Munroe Effect to cut metal plating, etc. The Munroe Effect states that an explosive charge may be shaped such that a linear cutting jet may be formed upon firing. Modern LSC consist of V-shaped metallic tubing containing plastic explosive. Current usage is aerospace rocket booster separation, etc.

Pyrotechnic vibration testing consists of simulated testing such as hammer tests, shaker tables, drop tests, high intensity shock machines, and others; and explosive testing such as actual flight monitoring, ground test of flight hardware, plate tests, barrel tests, and others. Shock data is collected by accelerometers and stress-strain measuring devices. Raw data is in the form of time histories. This data is analyzed to yield shock response spectra and Fourier spectra.

Shock or shock effects may be reduced by reducing the shock source, isolating the shock source, increasing the attenuation of the shock, using shock mounts, or by modifying or redesigning the equipment receiving the shock damage.

The "Aerospace Systems Pyrotechnic Shock Data" report is still state-of-the-art. The design criteria guidelines, described within it, are still used.

IX. CONCLUSIONS

1) Definition of pyrotechnic shock environments is still an empirical procedure.

2) LSC cutting ability as a function of LSC shape has improved over the past two decades.

3) Instrumentation for testing, measuring, and analyzing LSC induced pyroshock has improved over the last 20 years.

4) The seven volume report prepared for NASA by Martin Marietta in 1970 is still state-of-the-art.

5) No new data analysis techniques have been formulated.

6) A given shock response spectrum is not unique to a given shock transient.

7) To achieve an accurate pyroshock test, use a pyrotechnic source rather than a simulation. Most simulation tests achieve the proper SRS, but do not achieve the correct time histories.

8) Future research needs to be conducted to determine variations in SRS as functions of charge shape, charge coreload, and test instrumentation. SRS variation, due to LSC manufacturing tolerances, needs to be examined to prevent future hardware failures.

BIBLIOGRAPHY

1. Albers, L., "Pyrotechnic Shock Measurement and Data Analysis Requirements," JPL, IES.

2. Albers, L., "Pyrotechnic Shock Measurement and Data Analysis Requirements," Proc. IES, Volume II, 1975, pp. 11-18.

3. Albers, L., "Pyrotechnic Shock Measurement and Data Analysis Requirements - for Mariner Jupiter - Saturn 1977 Hardware," IES, 1975, pp. 3-47 to 3-68.

4. Bai, M., and Thatcher, W., "High G Pyrotechnic Shock Simulation Using Metal-to-Metal Impact," SVB, Part 1, pp. 91-100, September 1979.

5. Balog, E. M., "Upper Stage Systems Separation," Test Report, Boeing, Seattle.

6. Barrett, S., "The Development of Pyro Shock Test Requirements for Viking Lander Capsule Components," IES, 1975, pp. 5-10.

7. Barrett, S., and Kacena, W. J., "Techniques for Reducing Shock in Pyrotechnic Devices," SVB No. 42, Part 4, pp. 21-32, January 1972.

8. Belgrano, C., "Explosives," GLI Explosivi, 1974.

9. Bement, L. J., "Monitoring of Explosive/Pyrotechnic Performance," Franklin Institute, 1971, pp. II-1-1 to II-1-8.

10. Bouloumie, J. P., "European Pyrotechnic Devices Catalog for Use in Space Applications," ESA.

11. Bouloumie, J. P., Yribarren, J. P., and Cable, N., "Catalog of European Pyrotechnic Devices for Use in Space," ESA.

12. Brauer, K. O., "Pyrotechnic Devices and Pyrotechnic Systems for Spacecraft," ASWA, 1977, pp. 39-49.

13. Bucciarelli, L. L., and Askinazi, J., "Pyrotechnic Shock Synthesis Using Nonstationary Broad Band Noise," ASME, 1972.

14. Burker, W. R., and Mort, J., "Explosives and Pyrotechnics: Space Applications - Conference Proceedings," 1979.

15. Conference on Modern Applications of Pyrotechnics, June 1973.

16. Conway, J. J., Pugh, D. A., and Sereno, T. J., "Pyrotechnic Shock Simulation," IES, 1976, pp. 12-16.

17. Conway, J. J. and Sereno, T. J., "Pyrotechnic Shock Testing of Components," IES, 1977, pp. 109-112.

18. Draley, E. C., RTOP, NASA/Langley, 71W70684.

19. Dupont Explosive Specialities, Catalog.

20. Eighteen Mission Pyrotechnic Shock Certification Test of the SRB Integrated Receiver Decoder (IRD), NASA Internal Memorandum, December 1, 1983.

21. Engelsgferd, I. K. and Rader, W. P., "Aerospace Systems Pyrotechnic Shock Data/Ground Test and Flight," Volume 7, Martin Marietta, May-November 1970.

22. Ensign-Bickford Co., Explosive Specialities Catalog, 1980.

23. Ensign-Bickford Co., Catalog, 1970.

24. Environmental Technology '76: Proceedings of the Twenty-Second Annual Technical Meeting, April 1976.

25. Falbo, M. J., "Explosive and Pyrotechnic Devices in Spacecraft Systems," NASA/JSC, TM-X-72324.

26. Falbo, J. M. and Robinson, R. L., "Apollo Experience Report on Use of Pyrotechnic Devices in Systems of Apollo Spacecraft," NASA/JSC.

27. Fandrich, R. T. Jr., "Bounded Impact - A Repeatable Method for Pyrotechnic Shock Simulation," SVB No. 46, Part 2, 1976, pp. 101-107.

28. Fandrich, R. T. Jr., "Pyrotechnic Shock Testing on a Standard Drop Machine," 20th Annual Meeting, IES, 1974, pp. 269-273.

29. Graves, T. J., "Space Shuttles: A Pyrotechnic Overview," NASA/JSC.

30. Hieber and Tustin, "Understanding the Shock Response Spectrum," Sound and Vibration, March 1974, pp. 42-54.

31. Kacena, W. J., McGrath, M. B., and Rader, W. P., "Aerospace Systems Pyrotechnic Shock Data - Ground Test and Flight," Volume 1, Martin Marietta Corp., March 1970.

32. Kacena, W. J., McGrath, M. B., and Rader, W. P., "Aerospace Systems Pyrotechnic Shock Data - Ground Test and Flight," Volume 2, Martin Marietta Corp., March 7, 1970.

33. Kacena, W. J., McGrath, M. B., and Rader, W. P., "Aerospace Systems Pyrotechnic Shock Data - Ground Test and Flight," Volume 3, Martin Marietta Corp., March 7, 1970.

34. Kacena, W. J., McGrath, M. B., and Rader, W. P., "Aerospace Systems Pyrotechnic Shock Data - Ground Test and Flight," Volume 4, Martin Marietta Corp., March 7, 1970.

35. Kacena, W. J., McGrath, M. B., and Rader, W. P., "Aerospace Systems Pyrotechnic Shock Data - Ground Test and Flight," Volume 5, Martin Marietta Corp., March 7, 1970.

36. Kacena, W. J., McGrath, M. B., and Rader, W. P., "Aerospace Systems Pyrotechnic Shock Data - Ground Test and Flight," Volume 6, Martin Marietta Corp., March 7, 1970.

37. Keegan, W. B. and Bangs, W. F., "Effects of Various Parameters on Spacecraft Separation Shock," SVB No. 42, Part 3, January 1972, pp. 131-148.

38. Keller, Pollard, and Andress, "Shock Spectrum Analysis and Structural Design," 1973.

39. Labarge Electrical Cabels, Six Mission Pyrotechnic Shock Certification Test, NASA Internal Memorandum, November 9, 1983.

40. Larue, P., Millet, M., and Piazyoliz, G., "Pyrotechnic Pulse Generators for In-Flight Structural Tests," La Recherche Aerospatiale, 1974, pp. 137-146.

41. LeMay, C., "Actual and Predicted Reliability in Aerospace Pyrotechnics," 1979.

42. Lieberman, P., "Pyrotechnic Plate Analysis and Test Results — of Missile and Space Vehicle Hardware," International Instrumentation Symposium, 25th, May 1982.

43. Love, E. S., RTOP, NASA/Langley, 74W70302.

44. Luhrs, H. N., "Equipment Sensitivity to Pyrotechnic Shock," IES, 1976, pp. 3-4.

45. Luhrs, H. N., "Pyrotechnic Shock Testing - Past and Future," IES, Annual Technology Meeting, May 1981, pp. 17-20.

46. Luhrs, H. N., "Pyrotechnic Shock Transmission in Component Versus S/C Testing — Vibration Table Compared with Instrumented Spacecraft Model," IES 1975, pp. 3-27 to 3-44.

47. Marshall Space Flight Center Vibration Manual, Internal Note, 1968.

48. Mas, C., "Shock Waves: Knowledge, Use, and Protection," ESA.

49. Mas, C., "Shock Waves: How to Recognize Them, Use Them, and To Provide Against Them — Aerospace Structures," 1979.

50. McCormick-Selph Co., Technical Design Data, Catalog.

51. McGrath, M. B., "A Discussion of Pyrotechnic Shock Criteria," SVB No. 41, Part 5, December 1970.

52. McGrath, M. B., "Development of Criteria for Predicting Pyrotechnic Shock Environments and Spectra Found Near Source of Pyrotechnic Action," SVB No. 41, Part 5, pp. 1-7.

53. Mechanical Vibration and Shock Measurements, Bruel and Kjaer, a handbook.

54. Meeks, P. J., RTOP, JPL, 74W70303.

55. Milder, G. and Albers, L., "Miniature Pyrotechnic Shock Simulator — for Testing on Spacecraft," ISA, 1975, pp. 405-414.

56. Mitron Research Report No. CR60581, December 1964.

57. Nelson, D. B. and Prasthofer, P. H., "A Case for Damped Oscillatory Excitation as a Natural Pyrotechnic Shock Simulation," SVB No. 44, Part 3, August 1974, pp. 57-71.

58. Nelson, C. H., RTOP, NASA/Langley, 73W70289.

59. Neubert, V. H. and Parker, R. P., "High Frequency Shock of Spacecraft Systems," Final Report, NASA CR-128237.

60. Neubert, V. H. and Parker, R. P., "Timewise Output of Pyrotechnic Bolts," SVB, No. 44, Part 3, August 1974, pp. 101-110

61. Parker, R. P., Neubert, V. H., "High Frequency Response of Beams," Journal of Applied Mechanics, Volume 42, December 1975, pp. 805-808.

62. Petino, G. Jr., and Taylor, F. R., "Propagation and/or Detonation Tests of Pyrotechnic Compositions," Hazards Research Corp.

63. Pohlen, J. F., "Viking Lander Dynamics," SVB No. 44, Part 2, August 1974, pp. 41-46.

64. Powers, D. R., "Development of a Pyrotechnic Shock Test Facility," SVB No. 44, Part 3, August 1974, pp. 73-82.

65. Powers, D. R., "Simulation of Pyrotechnic Shock in a Test Laboratory," Environmental Tech '76, IES, pp. 5-9.

66. Prescott, S. N., "Investigation of Pyrotechnic Shock — for Spacecraft Structural Tests," ISA, 1974, pp. 181-185.

67. Prescott, S. N., "Pyrotechnic Shock Reduction," SVB No. 44, Part 3, August 1974, pp. 111-124.

68. Proceedings of the 5th International Pyrotechnics Seminar, 1976.

69. Proceedings of the 41st Symposium on Shock and Vibration, SVB No. 41, Part 5, 1970.

70. Rader, W. P. and Bangs, W. F., "A Summary of Pyrotechnic Shock in the Aerospace Industry," SVB No. 41, Part 5, December 1970.

71. Rader, W. P. and Bangs, W. F., "Pyrotechnic Test Simulation Techniques and Guidelines for Design and for Predicting Shock Environments," SVB No. 41, Part 5, pp. 9-15.

72. Rader, W. P., "Pyrotechnic Shock Sources and Environments," Environmental Tech '76, IES, pp. 1-2.

73. Random House College Dictionary, Random House Publishers, 1968.

74. Roberts, W. H., "Explosive Shock," SVB No. 40, Part 2, December 1969, pp. 21-30.

75. Rogers, W. F., Grissom, D. D., and Rhodes, L. R., "Pyrotechnic Shock at the Orbiter/External Tank Forward Attachment," Johnson Space Center, 11th Space Simulation Conference, pp. 33-42.

76. Rogers, W. F., "Space Shuttle Separation Mechanisms," NASA, JSC.

77. Salyer, R. A., "Development and Application of a High-Intensity Shock Machinem," Proc. IES, 1974, pp. 30-35.

78. Sayama, F. J., and Whitt, J. B., "EDESS: An Electromagnetically-Driven Explosive-Shock Simulator," SVB No. 51, Part 2, May 1981, pp. 137-147.

79. Schoessow, T. D., "Deviation of Shock Environmental Criteria — Characteristics of Barrel Tester for Shock Test Environment Generation."

80. Schumacher, C. A., "Three-Dimensional Vibration Fixture," Martin Marietta Corp.

81. Skidlovaskii, A. A., "Principles of Pyrotechnics," 1964, pp. 1-339.

82. Simmons, W. H., "Apollo Spacecraft Pyrotechnics," Franklin Institute, 1969.

83. Simmons, W. H., "Apollo Spacecraft Pyrotechnics," SAE, 1970.

84. Smallwood, David O., "An Improved Recursive Formula for Calculating Shock Response Spectra," SVB No. 51, Part 2, May 1981, pp. 211-217.

85. Smith, L. G., "Specification and Simulation of Pyrotechnic Environments," SAE No. 740805, 1974, pp. 1-5.

86. Snell, R. F., "Study of an Experimental Technique for Application to Structural Dynamic Problems," SVB No. 44, Part 3, August 1974, pp. 82-100.

87. SRB Frustum/Forward Skirt Separation Tests Shock Data, NASA, Unpublished.

88. Symposium on Explosives and Pyrotechnics, Proceedings of the 9th, Franklin Institute, 1976.

89. Symposium on Explosives and Pyrotechnics, 10th, February 1979.

90. Symposium on Explosives and Pyrotechnics, 11th, September 1981.

91. Trummel, M., "Specification of Pyro Shock Tests," Environmental Tech. '76, IES, pp. 10-11.

92. Two Mission Pyrotechnic Shock Certification Test of the SRB Integrated Receiver Decoder (IRD), NASA Internal Memorandum, November 29, 1983.

APPROVAL

PYROTECHNIC SHOCK: A LITERATURE SURVEY OF THE LINEAR SHAPED CHARGE (LSC)

By James Lee Smith

The information in this report has been reviewed for technical content. Review of any information concerning Department of Defense or nuclear energy activities or programs has been made by the MSFC Security Classification Officer. This report, in its entirety, has been determined to be unclassified.

for G. F. McDONOUGH
Director, Systems Dynamics Laboratory

☆ U.S. GOVERNMENT PRINTING OFFICE 1984—746-070/236